Neurobiology of Disease 187 (2023) 106320

Contents lists available at ScienceDirect

Neurobiology of Disease

journal homepage: www.elsevier.com/locate/ynbdi

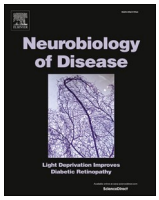

Potential role of *Bcl2* in lipid metabolism and synaptic dysfunction of age-related hearing loss

Yue Liu [a,b], Huasong Zhang [b,c,d,*], Cong Fan [d], Feiyi Liu [d], Shaoying Li [d], Juanjuan Li [b], Huiying Zhao [d], Xianhai Zeng [a,b,*]

[a] Department of Graduate and Scientific Research, Zunyi Medical University Zhuhai Campus, Zhuhai 519041, China
[b] Department of Otolaryngology, Longgang E.N.T Hospital & Shenzhen Key Laboratory of E.N.T, Institute of E.N.T, Shenzhen 518172, China
[c] Department of Otolaryngology, The Third Affiliated Hospital of Guangzhou Medical University, Guangzhou, 510000, China
[d] Department of Medical Research Center, Sun Yat-sen Memorial Hospital, Sun Yat-sen University; Guangdong Provincial Key Laboratory of Malignant Tumor Epigenetics and Gene Regulation, Guangzhou, 510000, China

ARTICLE INFO

Keywords:
Age-related hearing loss
Bcl2
Lipid metabolism
Synaptic dysfunction
Neuropathy

ABSTRACT

Age-related hearing loss (ARHL) is a prevalent condition affecting millions of individuals globally. This study investigated the role of the cell survival regulator *Bcl2* in ARHL through in vitro and in vivo experiments and metabolomics analysis. The results showed that the lack of *Bcl2* in the auditory cortex affects lipid metabolism, resulting in reduced synaptic function and neurodegeneration. Immunohistochemical analysis demonstrated enrichment of Bcl2 in specific areas of the auditory cortex, including the secondary auditory cortex, dorsal and ventral areas, and primary somatosensory cortex. In ARHL rats, a significant decrease in Bcl2 expression was observed in these areas. RNAseq analysis showed that the downregulation of *Bcl2* altered lipid metabolism pathways within the auditory pathway, which was further confirmed by metabolomics analysis. These results suggest that *Bcl2* plays a crucial role in regulating lipid metabolism, synaptic function, and neurodegeneration in ARHL; thereby, it could be a potential therapeutic target. We also revealed that *Bcl2* probably has a close connection with lipid peroxidation and reactive oxygen species (ROS) production occurring in cochlear hair cells and cortical neurons in ARHL. The study also identified changes in hair cells, spiral ganglion cells, and nerve fiber density as consequences of *Bcl2* deficiency, which could potentially contribute to the inner ear nerve blockage and subsequent hearing loss. Therefore, targeting *Bcl2* may be a promising potential therapeutic intervention for ARHL. These findings provide valuable insights into the molecular mechanisms underlying ARHL and may pave the way for novel treatment approaches for this prevalent age-related disorder.

1. Introduction

Age-related hearing loss (ARHL) is a highly prevalent condition among the elderly, characterized by peripheral hearing impairment and central neuropathy, which is associated with cognitive dysfunction and serves as a potentially modifiable risk factor for pre-dementia and Alzheimer's disease (AD) (Panza et al., 2015). The prevalence of significant hearing loss (pure tone thresholds averaging 0.5–4.0 kHz > 25 dB HL) in individuals aged 60–80 years is approximately 21–27%, and ARHL affects approximately 63.1% of people over 70 years of age in certain regions (Gopinath et al., 2009; Hogan et al., 2009; Lin et al., 2011). Substantial evidence suggests that ARHL has detrimental effects on the physical and mental health of the elderly and may serve as an early indicator of dementia and AD (Cherko et al., 2016; Cosetti and Lalwani, 2015; Taljaard et al., 2016). Therefore, understanding the underlying molecular mechanisms of ARHL is imperative for exploring therapies and interventions to mitigate ARHL and the potential risk of dementia.

In addition to sensorineural hearing loss, ARHL is characterized by impaired audibility at higher frequencies (6000–8000 Hz) as an early symptom, which can lead to speech comprehension and cognitive disorders (Eeles et al., 2012; Panza et al., 2011; Robertson et al., 2013). Peripheral sensor damage is the primary pathology in the early stages of ARHL, while central auditory lesions become more pronounced in later stages (Panza et al., 2011; Panza et al., 2015). Apart from cochlear

* Corresponding authors at: Department of Otolaryngology, Longgang E.N.T Hospital & Shenzhen Key Laboratory of E.N.T, Institute of E.N.T, Shenzhen 518172, China.
E-mail addresses: 980574786@qq.com (Y. Liu), 764137782@qq.com (H. Zhang), zxhklwx@163.com (X. Zeng).

https://doi.org/10.1016/j.nbd.2023.106320
Received 30 July 2023; Received in revised form 25 September 2023; Accepted 6 October 2023
Available online 7 October 2023

pathological changes associated with ARHL, such as the loss of hair cells, spiral ganglion neurons, and atrophy of the stria vascularis, the decrease in the quantity of synaptic connections between sensory hair cells and auditory neurons is also thought to be involved in the pathological process of ARHL (Buran et al., 2010; Frisina et al., 2016; Moser and Starr, 2016). Studies have provided evidence linking hearing impairment in ARHL patients, as assessed by audiometric thresholds, to changes in brain morphology, including cortical thinning and reduced gray matter volume in the auditory cortex (Giroud et al., 2017; Ren et al., 2018; Rigters et al., 2017), and ARHL is inextricably linked to neural remodeling (Slade et al., 2020). However, the underlying mechanisms are not yet fully understood.

Research has demonstrated that the activity-dependent Bax-caspase signaling cascades, which are part of the BCL2 protein family, play a role

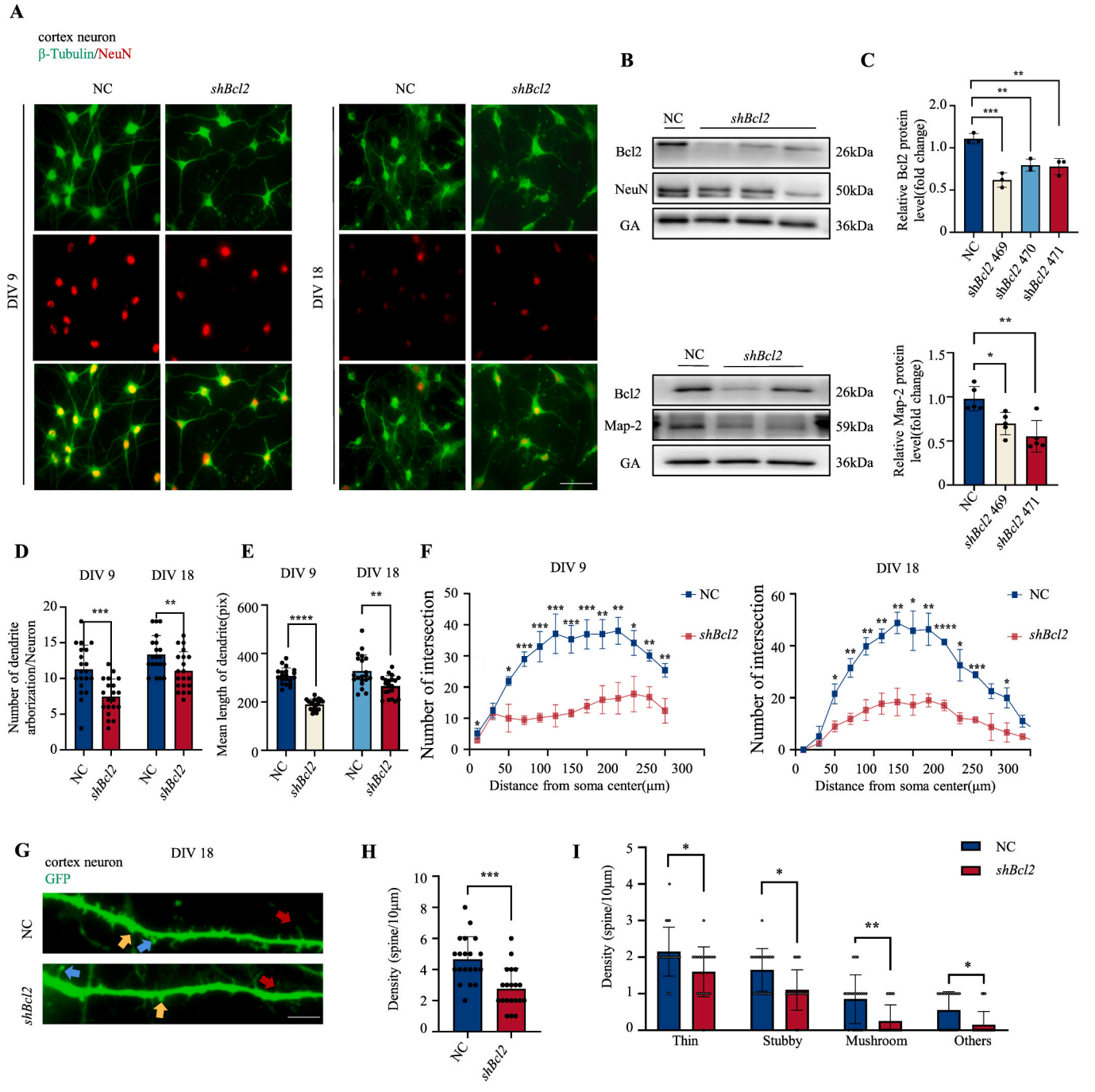

Fig. 1. *Bcl2* low expression significantly affects dendrite development in rat cortex neurons.
(A) Representative immunofluorescence images for β-Tubulin and NeuN (a marker for Neuronal nucleus) staining at DIV 9 and DIV 18. (B, C) Western-blot for Bcl2, Map-2, NeuN expression in *shBcl2* and control groups (Bcl2: $n = 3$, $p < 0.005$; Map-2: $n = 5$, *shBcl2* 469 $p = 0.0289$, *shBcl2* 471 $p = 0.0021$, One-Way ANOVA, Tukey post-hoc). (D, E) Number of dendrite arborization/neuron and mean length of dendrite were measured and quantified ($n = 20$ neurons. D, DIV 9: $p = 0.0003$, DIV 18: $p = 0.0150$, Student's *t*-tests). E, DIV 9: $p < 0.0001$, DIV 18: $p = 0.002$, Mann-Whitney *U* test). (F) Sholl analysis of dendritic branching at DIV 9 and DIV 18(n = 3, $p = 0.0005$ at DIV 9, $p < 0.0001$ at DIV 18; Two-Way ANOVA, Tukey post-hoc). (G) Representative images at DIV18 of dendritic spines in control and *Bcl2* shRNA with lentivirus transfected neurons by GFP staining. (H, I) The quantification data for the density and the number of spines. The color arrows pointed to different type of spines, stubby spine is yellow, thin spine is red, and mushroom spine is blue. (n = 20 neuron, $p < 0.05$ at DIV18, Mann-Whitney *U* test). Data represent mean ± SD.

not only in promoting the formation and reorganization of neural circuits but also in impacting synaptic and structural plasticity, indicating non-apoptotic function (S. Jiao and Li, 2011; Ohsawa et al., 2010; Simon et al., 2012). Bax/Bak-dependent caspase activation in descending corticospinal (CS) axons, which is dependent on neuronal activity, necessitates Bax/Bak (Nikolaev et al., 2009). Among the three members of the BCL2 protein family, which interact to facilitate BAX activation and function, leading to nerve injury (Gu et al., 2017). BCL2, an important factor that interacts with others, including BAX, to regulate apoptosis as well as participate in the inflammatory response (Delbridge et al., 2016), is also necessary for hearing development (Carpinelli et al., 2012). Research performed on gray matter structural covariance networks (SCNs) analysis and covariance strength has provided support for the influences of the Bcl-2 rs956572 functional polymorphism on the SCN in the early stage of AD (Chang et al., 2018). Bcl2 is critical in neuronal development and evidently decreases in the aging brain (Shimohama et al., 1998), and substantial evidence suggests it potentially linked to age-dependent neuronal remodeling, although the precise mechanism remains unclear. Among the genes of concern in the pathogenesis of ARHL, GRM7 (Friedman et al., 2009) and TRIOBP (Kalra et al., 2020) have been identified as risk loci associated with hearing difficulty. Based on these evidence, we will further explore the correlation between *Bcl2* and other genes with the disease process in ARHL.

In this study, we investigated the morphological and functional alteration of rats' auditory cortical neurons with *Bcl2* deficiency at different stages of development, along with the corresponding modification of neuronal synaptic remodeling and cytoskeleton development. Furthermore, by examining ARHL rats with age-related hearing impairment, we discovered similar patterns of altered plasticity in the cochlear with increasing an age-related deficiency of *Bcl2*. We propose that *Bcl2* affects cortex neuronal cytoskeleton formation and synaptic structural plasticity via the lipid metabolic pathway, including effects on cholesterol metabolism, lipid peroxidation, and ROS production, and plays an age-dependent role in auditory synaptic loss and neurodegeneration in ARHL. Our studies reveal the molecular mechanisms by which *Bcl2* participates in neural remodeling and the disease process of ARHL, providing the potential for using *Bcl2* as a new diagnostic indicator of ARHL and guiding clinical prevention strategies. These results provide new physiological and pathological insights into the development of ARHL and offer new possibilities for innovation in the therapies and prevention of ARHL.

2. Result

2.1. Impaired dendrite development in Bcl2 deficient neurons

To investigate the impact of *Bcl2* on neural plasticity, we examined the skeleton and dendritic morphology of cortical neurons in rats at different stages of neuron development. We selected DIV 9 to investigate early dendrite development, while later arborization and dendritic spine development were studied in neurons from DIV 14 to DIV 18 (Fig. 1A). Neurons were infected with *Bcl2* shRNA added after 24 h of culture and collected on DIV 9. Auditory cortex neurons were also treated with *Bcl2* shRNA after 10 days of normal culture, and then fixed on DIV 18 to imitate the neuron of the acquired Bcl2 reduction. Immunostaining results demonstrated delayed skeletal development of cortical neurons at different stages in the absence of Bcl2 compared to controls (silencing around 50% Bcl2 to avoid excessive apoptotic effects). We quantified the efficiency of Bcl2 expression in cultured rat cortical neurons by western blot and verified the reduction of Bcl2 (at least 50% reduction) in the *shBcl2* group ($p = 0.0004$). The expression of microtubule-associated protein-2 (Map-2) by western blot to reveal that levels are diminished in *shBcl2* neurons compared to control ($p = 0.0024$) (Fig. 1B, C). *Bcl2* depletion results in significant changes in dendrite number and length, apparent during both early and late stages, with *shBcl2* inducing the reduction of dendrite arborization ($p = 0.0003$, DIV 9 and $p = 0.0095$, DIV 18) and mean dendrite length in the *shBcl2* group of cortex neurons ($p < 0.0001$, DIV 9 and $p = 0.002$, DIV 18) (Fig. 1D, E). We analyzed the morphological diversity of cortical neurons with simplified dendritic arborization using Sholl analysis, and the *shBcl2* group was significantly differential compared to the normal control (NC) group ($p = 0.005$ and $p < 0.0001$) (Fig. 1F).

To delve deeper into age-related factors in depth, we focused on changes in neural plasticity when Bcl2 deletion commenced at DIV 11. At the end of the deficiency period, we quantified changes in dendritic spines and found significant differences in density per 10 μm stretches of dendrite between the two groups, and a remarkable decrease was present in the *shBcl2* group ($p = 0.0001$) (Fig. 1G, H). Among the different categories of dendritic spines, the silenced *Bcl2* group presented the most significant reduction in mushroom spines ($p = 0.0046$), followed by stubby spines and thin spines respectively ($p = 0.0089$ and $p = 0.0188$), and other spines (including long thin spines, filopodia spines and branched spines) also showed a slight decrease compared with the control group ($p = 0.0187$) (Fig. 1I). Taken together, these results demonstrated that *Bcl2* plays a significant role in dendritic development and influences the formation of dendritic branches and dendrites, at least within the constructed in vitro experiments.

2.2. Altered synaptic structure of shBcl2 neurons

To further elucidate the impact of *Bcl2* on synaptic structure and function, which is essential for neuronal communication in the cortex, we examined synapses containing synapsin I (SYN1) positive structures in cortical neural circuits. SYN1, the most abundant associated phosphoprotein in synaptic vesicles (SVs), has the ability to trap small lipid vesicles within its phase (Milovanovic et al., 2018). The absence of SYN1 has been shown to result in the dispersion of SVs both at rest (Pechstein et al., 2020) and upon depolarization (Pieribone et al., 1995). Notably, there was a significant reduction in SYN1 levels in *shBcl2* neurons starting at late synaptic development DIV10 until DIV18 compared to controls, which is similar to a substantial degree with age-related neurodegenerative disease. SYN1 decreased by 41.6% per 40 μm of dendrites in the *shBcl2* group, and the content of SYN1 on each neuron was reduced accordingly ($p < 0.0001$) (Fig. 2A-D). Previous research has proposed a mechanism whereby synapsin-mediated vesicle aggregation involves synaptophysins establishing a distinct liquid phase in the surrounding solution and being able to recruit lipid vesicles through their vesicle-binding activity. Phase separation associated with synapsins is potentially necessary for synaptic remodeling and maintenance (Milovanovic et al., 2018; Zeng et al., 2016). We have identified that *Bcl2* deficiency could induce the decrease in SYN1 in vitro. However, it remains unclear whether this could also affect the transport function of presynaptic vesicles and hinder the recruitment of lipid vesicles in cortical neurons. We displayed the immunofluorescence co-localization of SYN1 with the postsynaptic protein PSD95 in images to demonstrate the variation of the number and distribution in synapses shown in Fig. 2, and quantified that PSD95 decreased by 21.1% per 40 μm of dendrites in the *Bcl2*-silenced group as compared to the NC group ($p = 0.0182$) with the decrease level of PSD95 in each neuron ($p = 0.0014$) (Fig. 2E-G). All of the above results appropriately indicate that as *Bcl2* declines, the quantity of synapses in neurons declines, and synaptic structure is altered in vitro. To further elucidate the effects of *Bcl2* on ARHL cortical neurons. We split proteins from the auditory cortex of the brain of 8-month-old (8 M), 12-month-old (12 M), and 20-month-old (20 M) wild-type (WT) rats for Western blot experiments, in which 20 M rats were naturally aged and exhibited ARHL (Fig. 2H and Fig. 6C, D). Western blot showed that Bcl2, Map-2, PSD95, and SYN1 were decreased in the auditory cortex of ARHL rats compared with 8 M and 12 M WT rats ($p < 0.05$) (Fig. 2I). Validated with both in vivo and in vitro results, we identified that *Bcl2* is indeed intimately implicated in synaptic number and structure in ARHL.

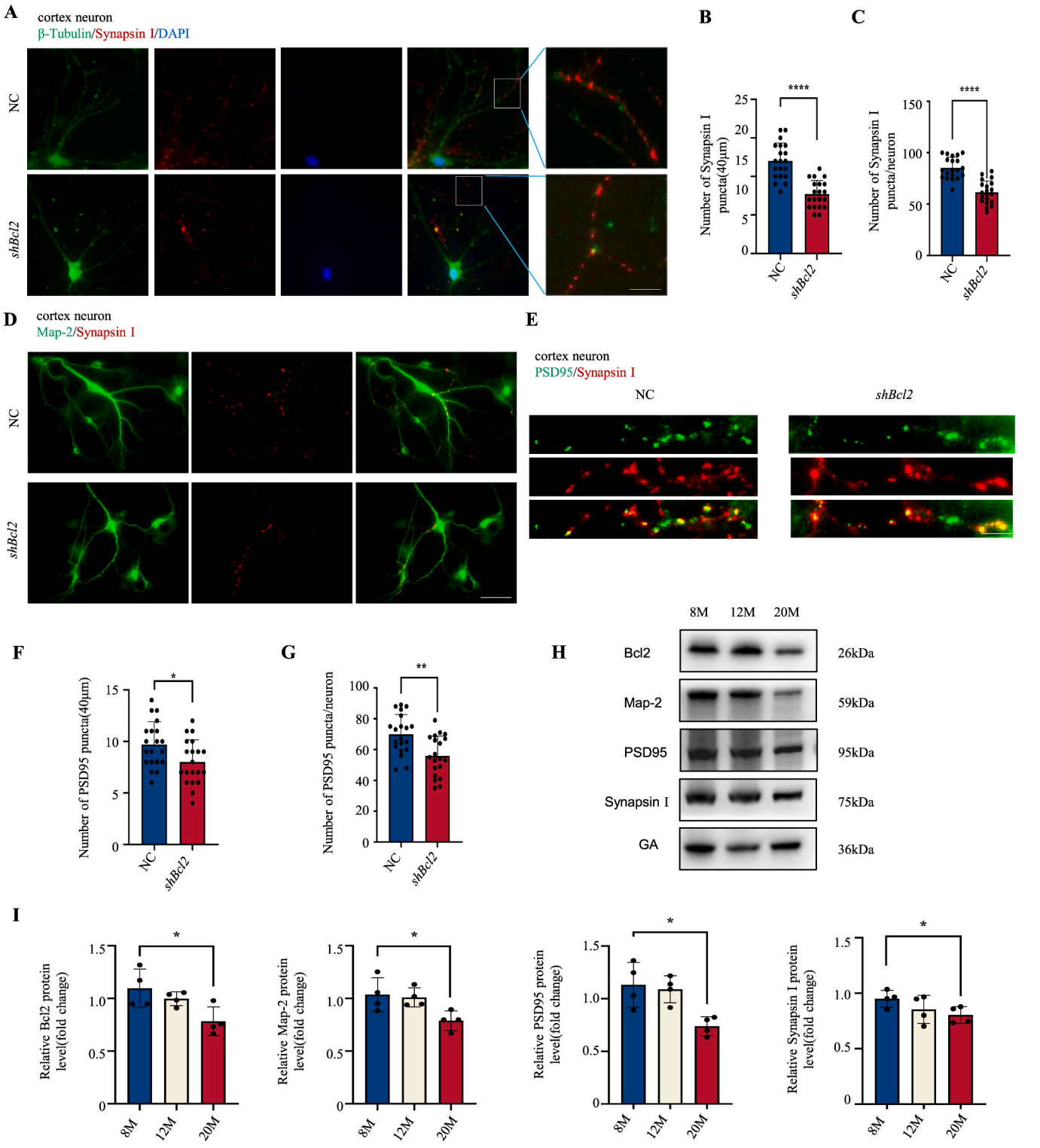

Fig. 2. *Bcl2* low expression significantly altered synaptic structure in rat cortex neurons.
(A) Representative immunofluorescence images for β-Tubulin, DAPI and SYN1 staining at DIV 18. (B, C) The quantification data for number of SYN1 puncta (40 μm) and number of SYN1 puncta/neuron(n = 20, $p < 0.0001$, Student's t-tests). (D, E) Representative immunofluorescence images for Map-2, PSD95 and SYN1 staining at DIV 18. (F, G) The quantification data for number of PSD95 puncta(40 μm) and number of PSD95 puncta/neuron(n = 20, $p = 0.0182$ and $p = 0.0014$, Student's test). (H, I) Western-blot for Bcl2, Map-2, PSD95 and SYN1 expression in brain auditory cortex of 8 M, 12 M and 20 M rats ($n = 4$, Bcl2: $p = 0.0273$, Map-2: $p = 0.0401$, PSD95: $p = 0.0239$, SYN1: $p = 0.0306$. One-Way ANOVA, Tukey post-hoc). Data represent mean ± SD.

2.3. Transcriptome analysis reveals potential involvement of Bcl2 in the pathogenesis of ARHL

Recent studies had showed that ARHL has been linked to neural remodeling that, in the context of age, correlates with synaptic disruption (He et al., 2023; Slade et al., 2020; Zhang et al., 2023). Our preliminary results, combined with previous studies, suggest that *Bcl2* potentially influences neural pathway remodeling and development. To explore the possibility of a direct relationship between *Bcl2* and disease progression in ARHL. Co-expression network analysis was performed to identify genes that showed similar expression patterns with *Bcl2*. The analysis revealed that *Bcl2* was perhaps potentially associated with ARHL (Fig. 3B), although the precise mechanism and signal pathway of interaction remained unknown. To investigate this further, *shBcl2* OC1 cells and a control group were subjected to transcriptome analysis using RNA-seq. Totally, 663 differentially expressed genes (DEGs) were

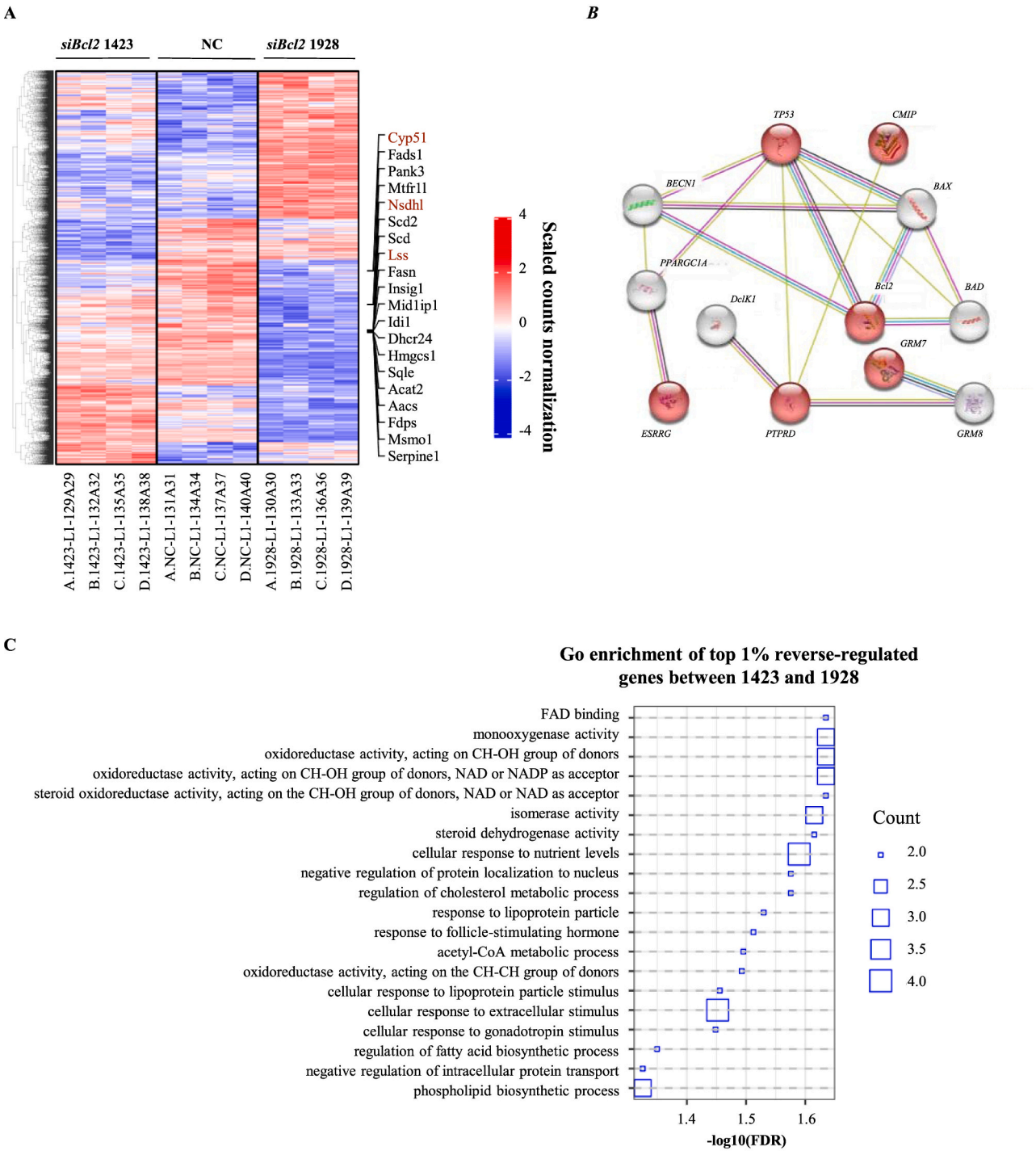

Fig. 3. *Bcl2* regulates ARHL-associated pathways.
(A) Heatmap for 663 differentially expressed genes ($p < 0.05$) in low expression group of *Bcl2* compared with control group. (B) Functionally associated gene clustering (STRING) identifies genes which related to age(red). (C) GO analysis indicated that up-and down-regulated genes primarily participated in the biological activities.

identified after screening, including up-regulated and down-regulated. Heatmap analysis showed that the DEGs were apparently enriched in Fdps, Aacs, Nsdhl, Lss and Cyp51 ($p < 0.05$) (Fig. 3A). Further Gene Ontology (GO) and Kyoto Encyclopedia of Genes and Genomes (KEGG) analysis revealed that the DEGs were significantly enriched in OC1 cell signaling pathways. Go enrichment of top 1% reverse-regulated genes in *Bcl2* silencing groups includes monooxygenase activity; oxidoreductase activity, acting on CH-OH group of donors; oxidoreductase activity, acting on CH-OH group of donors, NAD or NADP as an acceptor; steroid oxidoreductase activity, acting on the CH-OH group of donors, NAD or NAD as an acceptor and phospholipid biosynthetic process. Aside from the molecular pathways of lipid metabolism, such as steroid activity, a remarkable aspect is the lipid-related oxidative stress pathway induced by *Bcl2* silencing (Fig. 3C). Our results suggest that *Bcl2* is involved in the peripheral auditory system through its effects on lipid biosynthesis and that lipid metabolism is inevitably indispensable for hair cells. Additionally, a wide amount of evidence indicates that increased ROS production leads to lipid peroxidation, which disrupts membrane lipid asymmetry and may lead to changes in membrane fluidity, and fluidity is critical for efficient OHCs (Maulucci et al., 2014; Mykytczuk et al., 2007; Tekpli et al., 2013). Therefore, ROS-induced alterations in lipid composition and the thermodynamics of the plasma membrane could play an essential role in regulating OHC function (Chen and Zhao, 2007). In general, the obstruction of hair cell metabolism by *Bcl2* has the potential to significantly impact auditory signaling. However, further studies are required to elucidate the underlying mechanisms and signaling pathways.

2.4. Bcl2 effects cholesterol metabolism in the auditory cortex

We have previously shown that *Bcl2* deficiency leads to alterations in synaptic morphology and plasticity of auditory cortical neurons during aging and further verified the concrete mechanism of effect. Here, we aimed to investigate the specific mechanism underlying these effects in the context of ARHL. Cholesterol metabolism plays an essential role in various neurophysiological and neuropathological processes, including synaptogenesis, axonal growth, and dendrite development (Chevy et al., 2005; Pfrieger, 2003).

Immunoblotting and qPCR confirmed reduced expression of Lss, Nsdhl and Cyp51 in *Bcl2*-deficienct outer hair cells (OHCs) and neurons compared to control groups. Specifically, Lss and Cyp51 were most prominently decreased by 33.5% and 49.6% in OC1 cells that were reduced *Bcl2* compared with NC and Lss was lowered by 40.7% in the neurons ($p < 0.05$) (Fig. 4A-D). qPCR results indicated a 35.7% decrease in Nsdhl expression in OC1 cells, although it was not expressed at the protein level, which may be related to the cholesterol synthesis pathway ($p < 0.05$) (Fig. 4E).

To further investigate the potential role of *Bcl2* in cholesterol metabolism, we quantified the expression of cholesterol in OHCs and neurons using immunostaining with filipin III, a fluorescent chemical compound that binds to cholesterol. Immunofluorescence analysis revealed lower signals of filipin III in *shBcl2* neurons, with a 28.9% reduction compared to control (NC) groups ($p < 0.0001$) (Fig. 4F, G). These findings demonstrate that *Bcl2* may predispose to alterations of lipid metabolites in the auditory cortex, which further validates our previous speculation that *Bcl2* deficiency interferes with the metabolism of the auditory cortex.

2.5. Metabolomics reveals that Bcl2 silencing impairs lipid metabolism in auditory cortex neurons

We previously identified that Bcl2 may affect the expression of mRNA and proteins in the cholesterol metabolic pathway of neurons. To further investigate the metabolism and mechanisms by which *Bcl2* regulates synaptic plasticity in neurons, we conducted a metabolomic study using LC-MS on cell clusters consisting of co-cultured neurons and glial cells. We performed hierarchical clustering of samples across groups using qualitatively significant differences in metabolite expression and used heat maps to visually screen for higher relative expression of marker metabolites. The bubble diagram demonstrates the metabolic pathways that were statistically distinct in the *shBcl2* group compared to NC, with the size of the circles indicating the number of differential metabolites annotated to that pathway, with greater circles being more important, including bile Acids, fatty acids, phosphatidylacids, steroids, hormones and sphingolipids that were part of lipid metabolism. There are indeed distinct differences, with a *p*-value >0.05 for the *t*-test and a fold change greater than twofold when comparing between the *shBcl2* group and control (Fig. 5 A). As shown in image (Fig. 5B), in the *shBcl2* group, biomolecules involved in lipid metabolism together with metabolites in steroid metabolism, including 23-Nordeoxycholic acid, PE (P-18:2/18:2), SM 32:2;3 and beta-Hydroxymyristic acid, were significantly down-regulated compared to the NC group; additionally, CMA, GALA and Estradiol(E2) were up-regulated ($p < 0.05$). The colors (from blue to red) indicate a change from a decrease to an increase in relative expression. Notably, changes in the nerve sphingolipids are intimately attached to the physiological activity and function of neurons. The circos image showed that the association of differential metabolic pathways in the *shBcl2* group compared to the NC group is red for promotion, blue for inhibition (Fig. 5C). Based on the present observations, it is well established that *Bcl2* may contribute substantially to neuronal lipid metabolic pathways and have a role in cell membranes, synaptic structure, and transmission of signals, but the underlying mechanisms still remain to be explored.

2.6. Bcl2 deletion is associated with synaptic degeneration in the specific regions of the auditory cortex and cochlea

Immunohistochemistry analysis was performed to assess the expression of *Bcl2* in various brain regions, including the secondary auditory cortex, dorsal area (AUD), and ventral area (AUV), ventral lateral geniculate nucleus (vLGN), and primary somatosensory cortex (S1), in 8 M and 20 M rats. The results showed a significant decrease of Bcl2 content in these regions of 20 M rats, with a 41.8% reduction in positive area compared to 8 M rats ($p = 0.0087$) (Fig. 6E, F). To investigate the association between *Bcl2* deletion and synaptic density, we simultaneously quantified the level of Map-2, a marker for synaptic density, in these regions and the hippocampus and correlated it with age-dependent Bcl2 expression. Our findings revealed a significant correlation between Bcl2 deletion and a 45.6% reduction in synapses in the auditory cortex of the ARHL model ($p = 0.0022$) (Fig. 6G, H). These results suggest that the reduction of *Bcl2* may lead to synaptic changes in auditory transmission pathways, particularly in regions such as AUD within the cortex. Intramodal plasticity is another form of cortical plasticity in which brain changes are induced within specific cortical areas due to increased or decreased input from the sensory system. Auditory deprivation, such as hearing loss or deafness, may lead to cortical cross-modal plasticity, where auditory cortex is used for visual or somatosensory processing, while blindness leads to recruitment of the visual cortex for somatosensory (vibrotactile) and auditory processing (Allman et al., 2009; Buckley and Tobey, 2011; Kim et al., 2016; Stropahl et al., 2015).Some studies have observed the recruitment of auditory cortex to visuomotor processing using functional near-infrared spectroscopy (fNIRS) techniques (Shiell et al., 2016).Campbell and Sharma's results indicated that cross-modal recruitment of vision appears to occur in age-related mild-moderate hearing loss (Campbell and Sharma, 2014, 2016). In summary, our findings suggest that *Bcl2* is specifically associated with synaptic degeneration in the AUD, AUV and S1 of the auditory cortex in the context of ARHL. Further investigations are necessary to unravel the underlying mechanisms by which *Bcl2* influences synaptic density in these regions and its functional implications in ARHL.

Sensorineural hearing loss has been closely associated with the

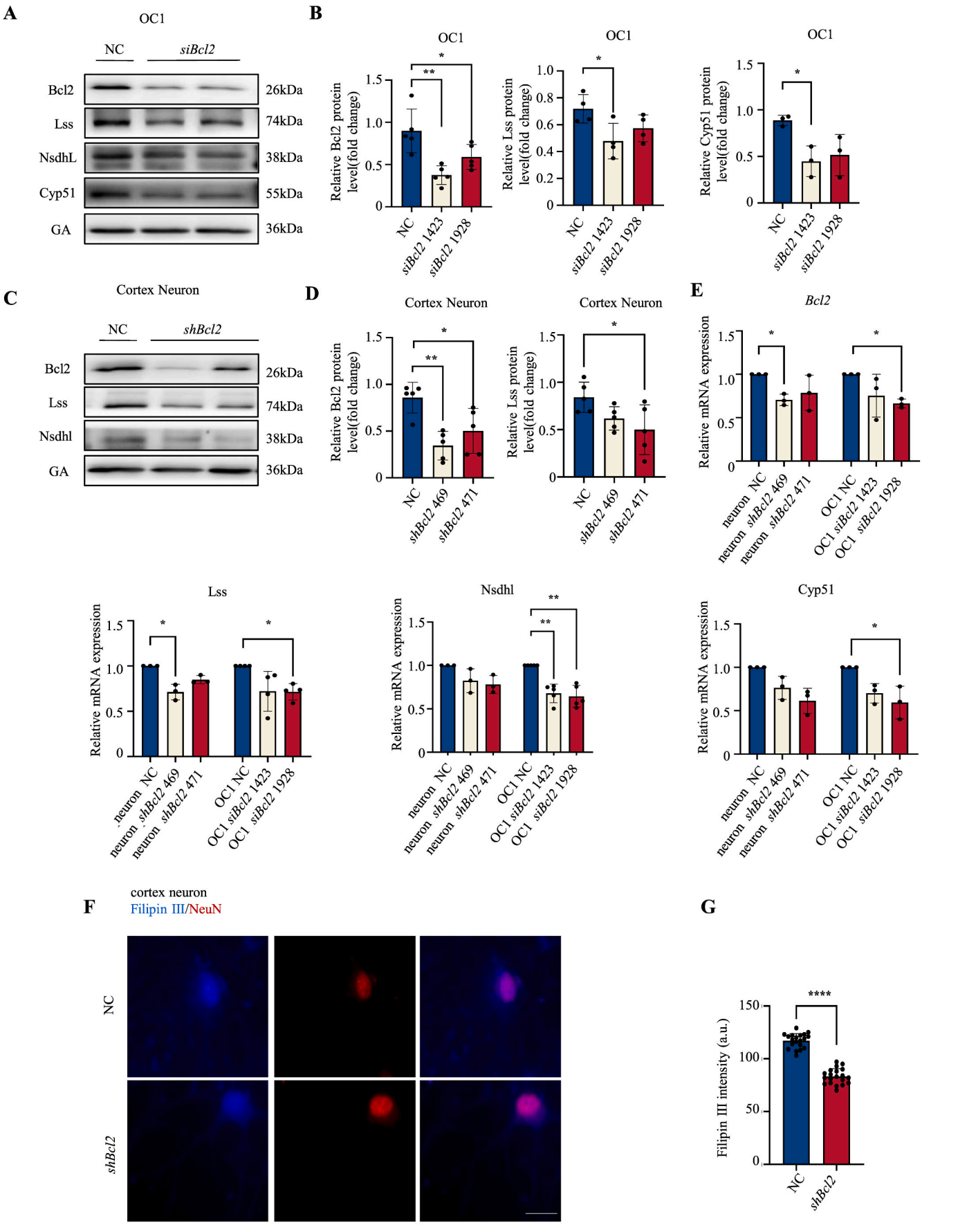

(caption on next page)

Fig. 4. Differential expression caused by *Bcl2* deficiency.
(A, B) Western-blot results for Bcl2, Lss, NsdhL and Cyp51 expression in *Bcl2* low-expression and control groups of OC1 cells ($n = 5$ or 4 or 3, Bcl2: *shBcl2* 469 $p = 0.0019$, *shBcl2* 471 $p = 0.0496$, Lss: *shBcl2* 469 $p = 0.0358$, Cyp51: shBcl2 469 $p = 0.0368$, One-Way ANOVA, Tukey post-hoc). (C, D) Western-blot results for Bcl2, Lss, Nsdhl expression in *Bcl2* low-expression and control groups of cortex neurons (n = 5, Bcl2: *shBcl2* 469 $p = 0.0028$, *shBcl2* 471 $p = 0.0292$, Lss: *shBcl2* 471 $p = 0.0373$, One-Way ANOVA, Tukey post-hoc). (E) qPCR results for Bcl2, Lss, Nsdhl and Cyp51 expression in *Bcl2* low-expression and control groups of OC1 cells and cortex neurons (n = 5 or 4 or 3, Bcl2: neurons *shBcl2* 469 $p = 0.0297$, OC1 *siBcl2* 1928 $p = 0.0141$, Lss: neuron *shBcl2* 469 $p = 0.0126$, OC1 *siBcl2* 1928 $p = 0.0163$, Nsdhl: OC1 *siBcl2* 1423 $p = 0.0057$, OC1 *siBcl2* 1928 $p = 0.0069$, Cyp51: OC1 *siBcl2* 1928 $p = 0.0318$, One-Way ANOVA, Tukey post-hoc) (F) Representative immunofluorescence images for FilipinIII staining at DIV 18. (G) The quantification data for FilipinIII intensity (a.u.) (n = 20, $p < 0.001$, Mann-Whitney *U* test). Data represent mean ± SD.

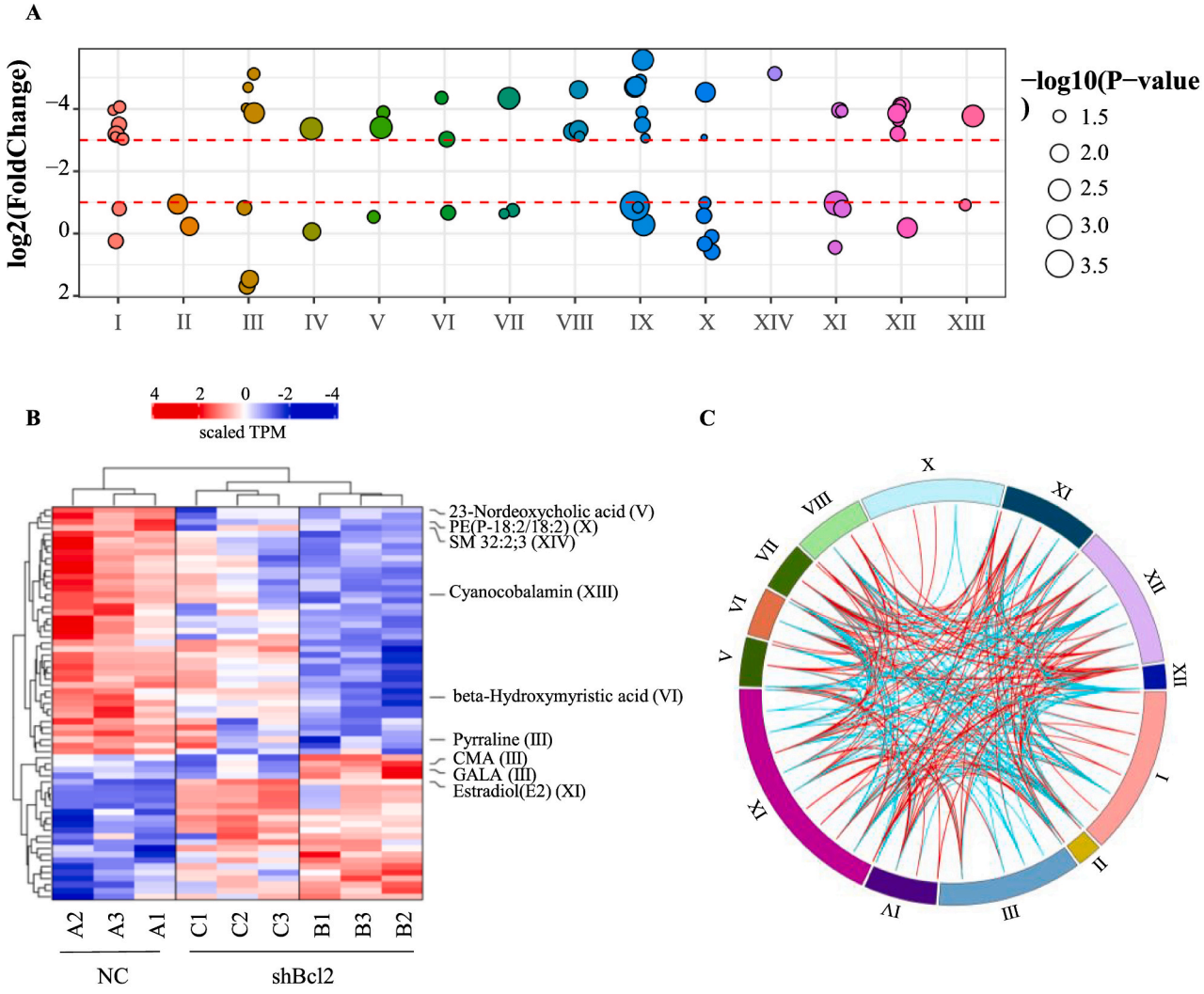

I - Acyl carnitines
II - Acyl glycerol
III - AGEs
IV - Amines,choline, and organonitrogen compounds
V - Bile Acids
VI - Fatty Acids
VII - Flavonoids, benzene and substituted derivatives
VIII - Indoles and heterocyclic compounds
IX - Organic acids and derivatives
X - Phosphatidylacids
XI - Steroids, hormones
XII - Sugar and derivatives
XIII - Vitamins and derivatives
XIV-Sphingolipids

Fig. 5. Metabolomics indicates that Bcl2 silencing hinders lipid metabolism in auditory cortex neurons.
(A) Heatmap for differential metabolites ($p < 0.05$) in low expression group of *Bcl2* compared with control group. (B) Bubble diagram for differential metabolic pathways ($p < 0.05$) in low expression group of *Bcl2* compared with control group. (C) Circos diagram for relevance of differential metabolic pathways ($p < 0.05$) in low expression group of *Bcl2* compared with control group. Data represent mean ± SD.

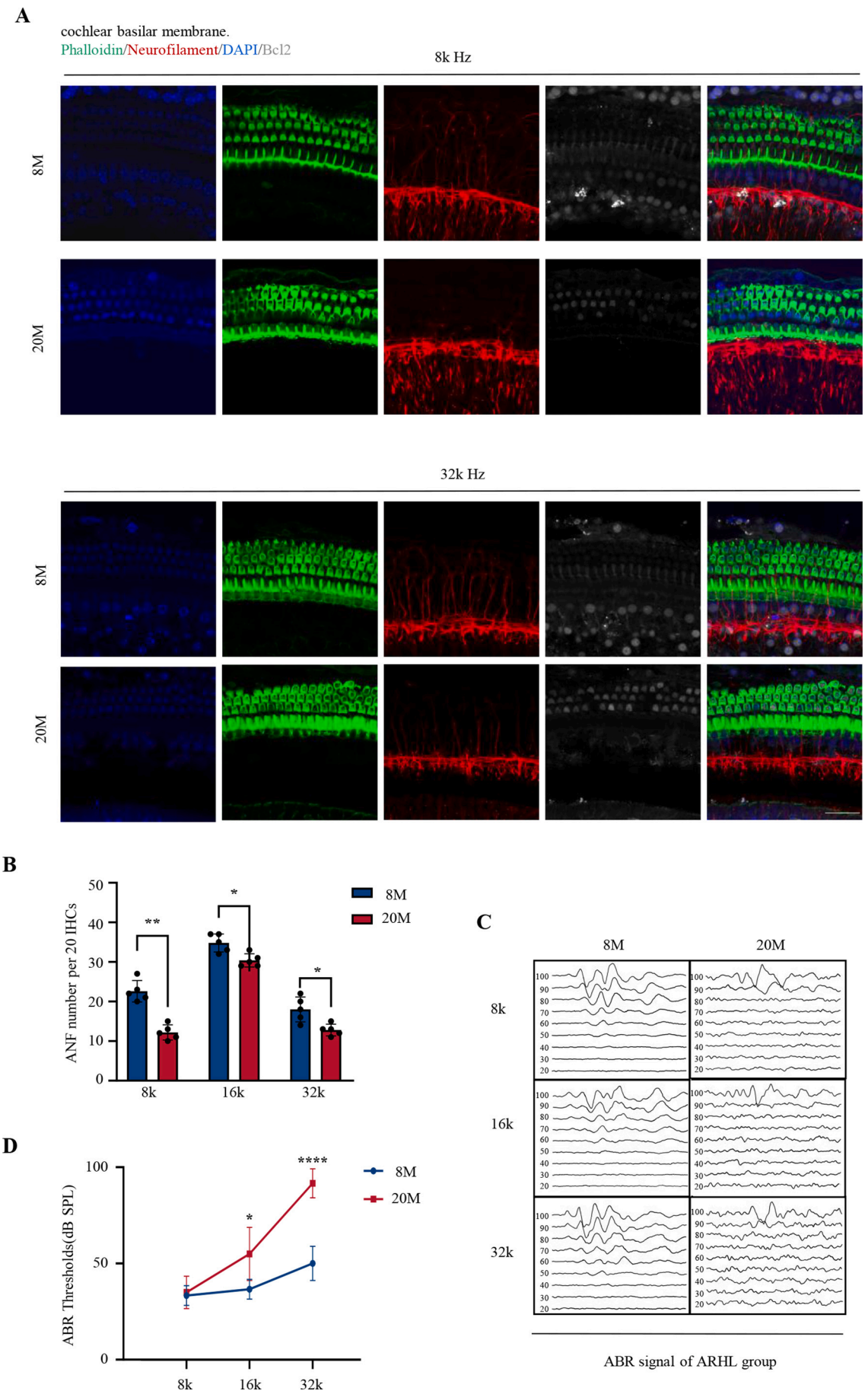
A
cochlear basilar membrane.
Phalloidin/Neurofilament/DAPI/Bcl2
8k Hz
8M
20M
32k Hz
8M
20M
B
ANF number per 20 IHCs
8M
20M
**
*
*
8k
16k
32k
C
8M
20M
8k
16k
32k
ABR signal of ARHL group
D
ABR Thresholds(dB SPL)
8M
20M
*
****
8k
16k
32k

Fig. 6. *Bcl2* deletion is associated with synaptic degeneration in specific region of the auditory cortex and cochlea.
(A) Representative immunofluorescence images for Phalloidin, Neurofilament 200, Bcl2 and DAPI staining of the cochlear basilar membrane in 8 M and 20 M rats. (B) The quantification data for ANF number which across 20 IHCs (n = 5 cochleae, 8 k, $p = 0.0079$. 16 k, $p = 0.0238$. 32 k, $p = 0.0159$, Mann-Whitney U test). (C) Typical changes in auditory brainstem response (ABR) signals over months. (D) The quantification data for ABR thresholds of 8 M and 20 M rats ($n = 6$ rats, 16kHZ $p = 0.0127$, 32kHZ $p < 0.05$, Two-Way ANOVA, Tukey post-hoc). (E, F, G, H) Immunohistochemical staining and quantification for significant synaptic changes in specific areas of the auditory cortex associated with Bcl2 (n = 6 rats, Bcl2: $p = 0.0087$ and $p = 0.0022$. Map-2: $p = 0.0022$, Mann-Whitney U test). Data represent mean ± SD.

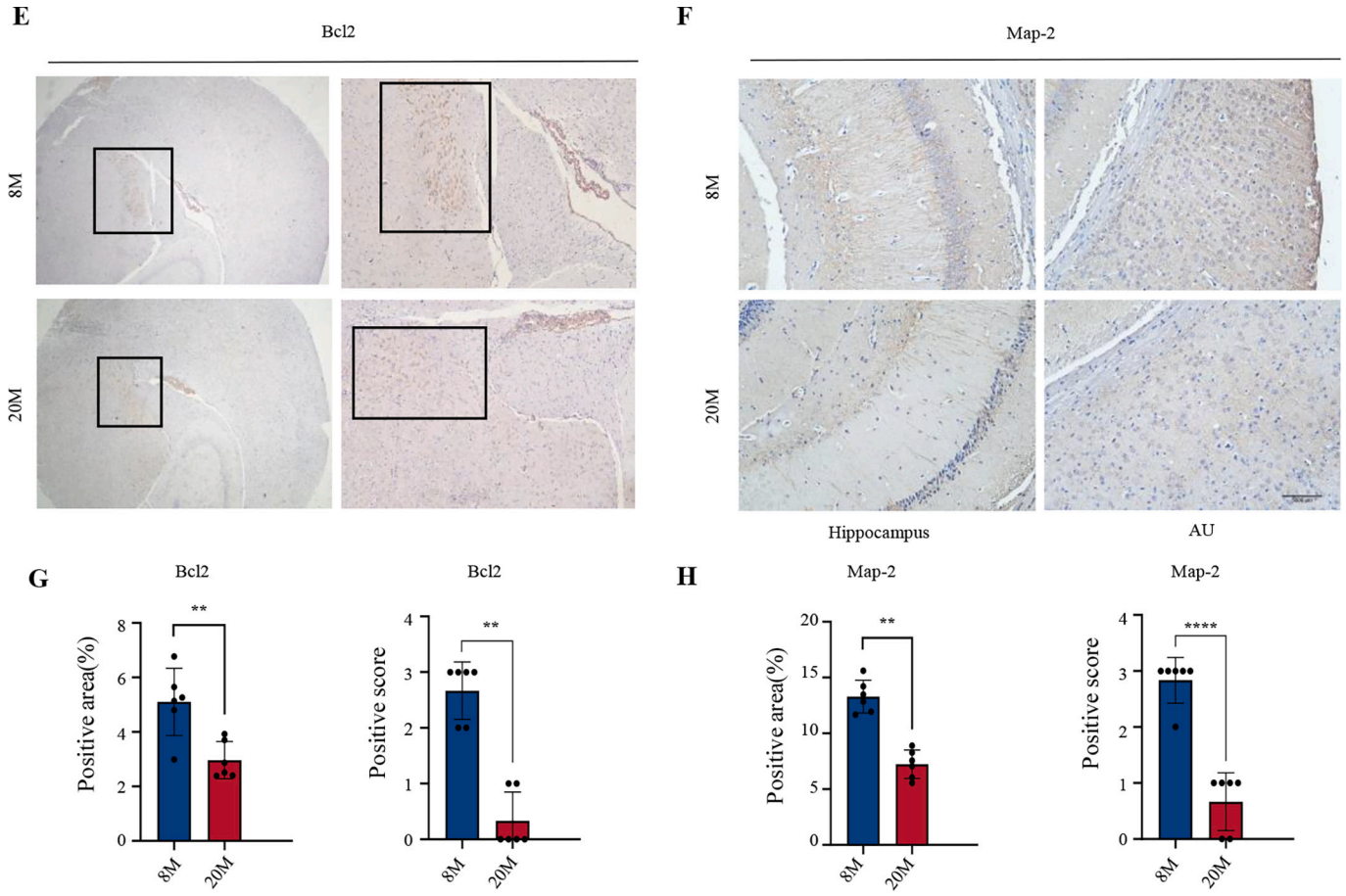

Fig. 6. (*continued*).

impairment of ribbon synapses in inner hair cells (IHCs) and synapses of spiral ganglion cells in the cochlea (Brandt et al., 2003; Rutherford et al., 2012). The Sprague-Dawley rat strains are frequently used as an animal model to research the potential mechanisms of ARHL (Keithley and Feldman, 1982; Sanz-Fernández et al., 2016). In Sprague-Dawley rats, scattered hair cell loss was found early in life and developed with age, as well as a marked decrease in spiral ganglion neuron (SGN) over time (Keithley and Feldman, 1982). In addition, the observation of activation of caspase3 and caspase8 as well as the increased expression of Bax proteins associated with the reduction of Bcl-xL proteins, supports the hypothesis that age-related apoptosis activates intrinsic pathways of pro-apoptotic signaling in the cochlea of Sprague-Dawley rats (Nevado et al., 2006), which is intimately linked to our work on the role of *Bcl2* in modulation of the ARHL potential mechanism. We performed immunofluorescence (IF) analysis on the cochlear basilar membrane of 8 M and 20 M WT rats as healthy controls, as well as the ARHL model (Fig. 6A and S2). We used 8 M rats with normal hearing as a control group and 20 M rats, who gradually began to experience hearing loss, to minimize the effect of later apoptosis on the study, as the senescent ARHL group, and we validated the results with auditory brainstem response (ABR) ($p < 0.05$) (Fig. 6C and D). We analyzed the expression of *Bcl2* in hair cells and spiral ganglion cells, quantified the length of nerve fibers originating from spiral ganglion cells, and counted the number of nerve fibers passing through per 20 IHCs. The analysis revealed a significant decrease of 46% and 28.9% in the number of ANF crossing the IHC at 8 kHz and 32 kHz in 20 M elderly rats with hearing loss, compared with young healthy rats, and no statistical change in ANF length ($p = 0.0079$ and $p = 0.0159$) (Fig. 6B). While impaired spike production in spiral ganglia or propagation along the SGN, as well as altered synaptic transmission from SGNs to neurons in the cochlear nucleus, ultimately leading to reduced auditory signal transmission to the brain. Loss of temporal accuracy (or synchrony) and inaccurate neural representation of the auditory signal are also key disease mechanisms in auditory synaptic disorders and neuropathies (Moser and Starr, 2016). We demonstrate that auditory synaptic dysfunction and neuropathy in ARHL during aging are also accompanied by a concomitant lack of *Bcl2*, as evidenced by the observed changes in hair cell, spiral ganglion cell, and nerve fiber densities. Further studies are required to elucidate the potential mechanisms by which *Bcl2* affects synaptic function and neuropathy in ARHL and to explore potential therapeutic interventions targeting *Bcl2* for the treatment of ARHL.

2.7. Modulation of lipid peroxidation by diminished Bcl2 in ARHL

Lipid peroxidation has been found to be associated with neurodegeneration (Dalleau et al., 2013; Di Domenico et al., 2017), and

combined with our RNAseq analysis of the *Bcl2* silencing group (Fig. 3), we assayed lipid peroxidation-related indicators to further detect the interaction between *Bcl2* and lipid peroxidation in ARHL. We performed ROS detection using the fluorescent probe Dihydroethidium (DHE) in living OC1 cells that reduced *Bcl2* by transfection compared to the NC group and found that the DHE fluorescence intensity in the *Bcl2* silencing group was 2.4 folds higher than that in the NC group ($p = 0.0022$) (Fig. 7A, B). Another assay indicator, 4-hydroxy-2-nonenal (4-HNE), was detected in OC1 cells and DIV9 neurons, which is one of the most abundant cytotoxic end products of lipid peroxidation (Awasthi et al., 2004). The graphs indicated that the content of 4-HNE in the *Bcl2* silencing group was higher than that in the NC group in OC1 by ELISA (*p*

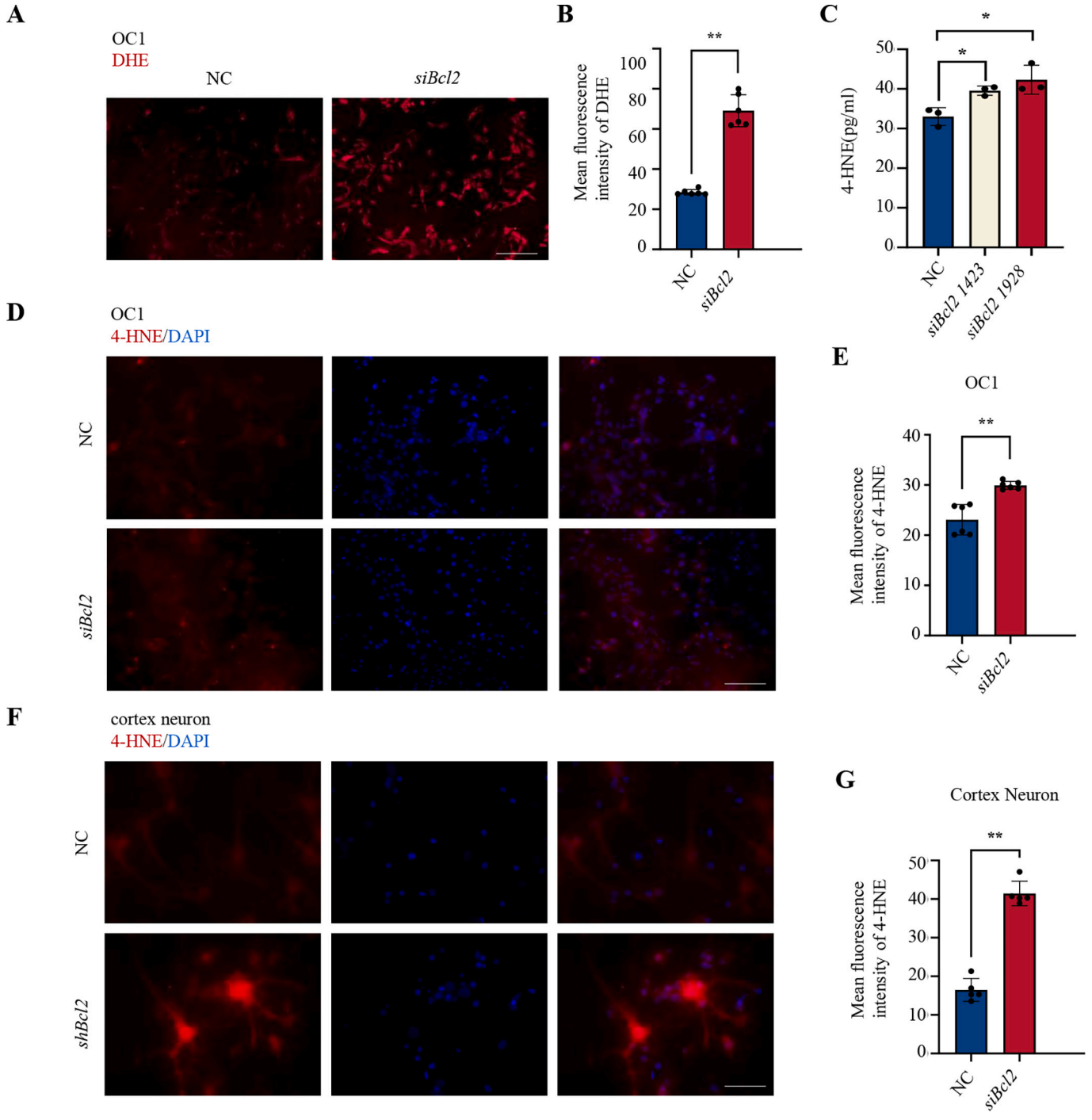

Fig. 7. Modulation of lipid peroxidation by diminished *Bcl2* in ARHL.
(A) Representative immunofluorescence images for DHE staining in living OC1 cells. (B) The quantification data for mean fluorescence intensity of DHE (n = 5, $p = 0.0022$, Mann-Whitney U test). (C) ELISA assay of 4-HNE in OC1 cells silenced *Bcl2* compared to the NC group ($n = 3$, $p = 0.0112$, One-Way ANOVA, Tukey post-hoc). (D, F) Representative immunofluorescence images for 4-HNE and DAPI staining in OC1 cells and DIV9 cortex neurons. (E, G) The quantification data for mean fluorescence intensity of 4-HNE ($n = 4$, OC1: $p = 0.0022$, cortex neuron: $p = 0.0079$, Mann-Whitney U test). (H) Representative immunofluorescence images for Phalloidin, 4-HNE and DAPI staining of the cochlear basilar membrane in 8 M and 20 M rats. (I) The quantification data for mean fluorescence intensity of 4-HNE (n = 4, $p = 0.0286$, Mann-Whitney U test). Apex: apical turn of cochlear base membrane. Middle: middle turn of cochlear base membrane. Base: base turn of cochlear base membrane.Data represent mean ± SD.

H

cochlear basilar membrane.
Phalloidin/4-HNE/DAPI

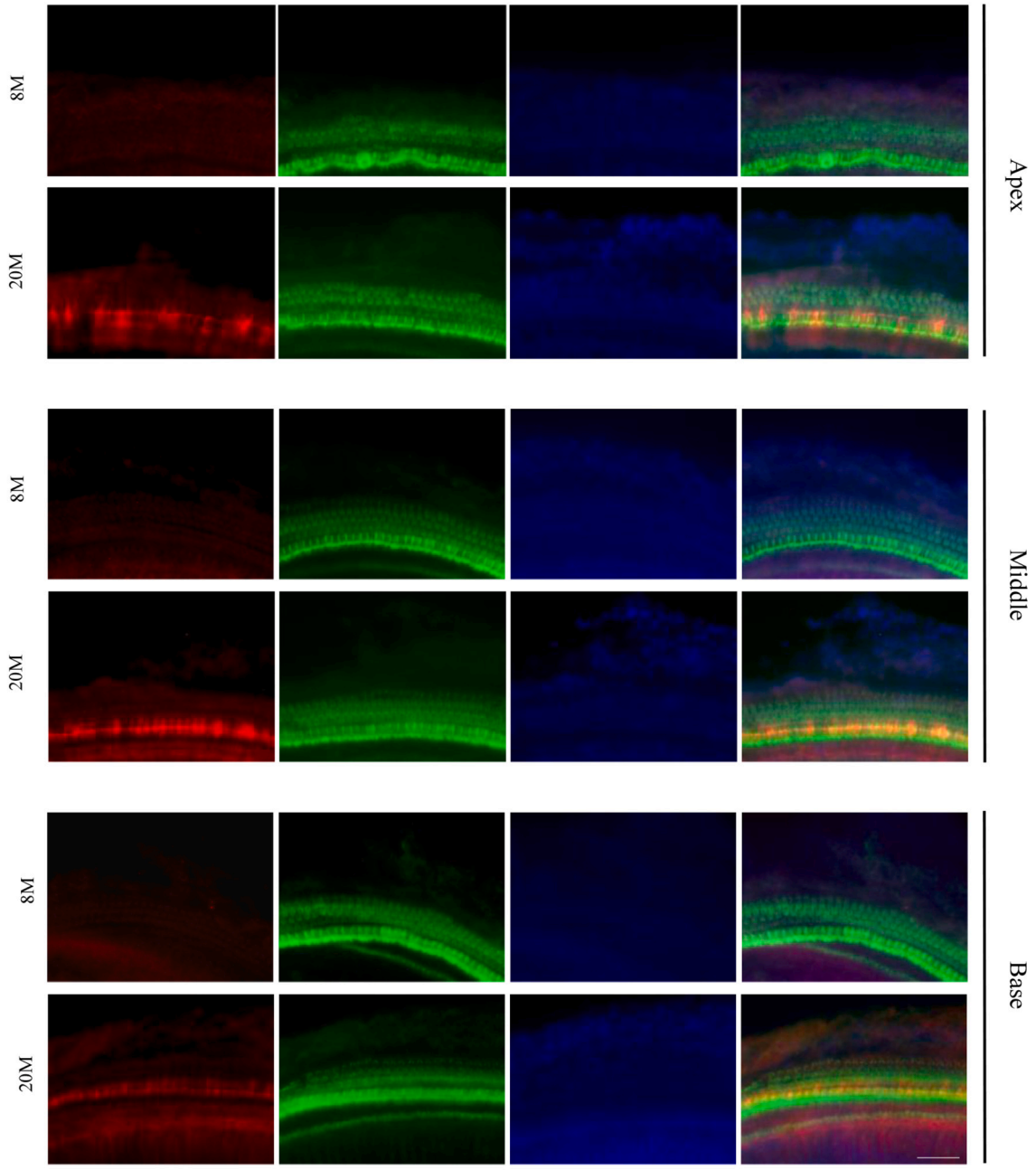

I

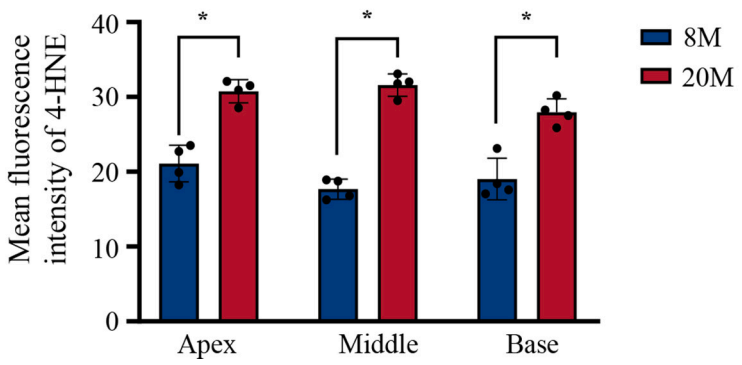

Fig. 7. (*continued*).

= 0.0198) (Fig. 7C), and the fluorescence intensity of 4-HNE in the *Bcl2* silencing group was higher than that in NC group in cortical neurons and OC1 ($p < 0.05$) (Fig. 7D-G). We also assayed 4-HNE production in the basilar membrane of the cochlea in 8 M WT rats and 20 M ARHL rats. We revealed that the 4-HNE of hair cells in the cochlea basilar membrane of ARHL rats was significantly raised, and the difference in fluorescence intensity of hair cells in the middle turn of the cochlear base membrane was the most obvious ($p < 0.05$), meanwhile, in both the apical turn and base turn of the cochlear base membrane, the 4-HNE protein content of the hair cells was measurably increased (Fig. 7H,I), which suggests that lipid peroxidation does exert a role in ARHL and that cytotoxic substances, such as 4-HNE produced by lipid peroxidation, will seriously affect the function of hair cells and cortical neurons and consequently obstruct the auditory pathway to promote ARHL.

3. Discussion

In summary, our study provides new insights into the molecular mechanisms underlying ARHL pathogenesis and identifies *Bcl2* as a key regulator of lipid metabolism, synaptic function, and neuropathy in this disorder. Our findings suggest that targeting *Bcl2* may hold promise as a potential therapeutic approach for treating ARHL. Furthermore, our study highlights the importance of investigating the role of lipid metabolism and synaptic dysfunction in the pathogenesis of ARHL, and further studies are warranted to elucidate the underlying mechanisms and explore potential therapeutic interventions. Future investigations could focus on delineating the specific signaling pathways through which *Bcl2* modulates lipid metabolism, synaptic function, and neuropathy in the auditory system. Ultimately, gaining a deeper understanding of the molecular mechanisms involved in ARHL may pave the way for the development of novel therapeutic strategies aimed at preventing or treating this debilitating condition.

Bcl2 deficiency impairs lipid metabolism in the auditory cortex, as shown in our metabolomic study. Our metabolomic study revealed significant alterations in lipid metabolic pathways in *Bcl2*-deficient OC1 cells and neurons compared to control groups, indicating the critical role of *Bcl2* in regulating lipid metabolism in the auditory cortex. This suggests that *Bcl2* may play a critical role in regulating lipid metabolism in the auditory cortex, which has important implications for various neurophysiological and neuropathological processes such as synaptogenesis, axonal growth, and dendrite development. Specifically, our results highlight the involvement of *Bcl2* on lipid metabolism, as evidenced by the down-regulation of genes in the cholesterol synthesis pathway and the observed staining patterns. These findings are consistent with previous studies emphasizing the crucial role of lipid, which is an important structural component of synaptic membranes and plays a crucial role in the development and maintenance of synapses (Chevy et al., 2005; Pfrieger, 2003). Studies by Barres BA et al. have demonstrated the requirement of cholesterol in the central nervous system for synaptic and dendrite formation, as well as its involvement in axon guidance and participation as a precursor in various biosynthetic pathways (Barres and Smith, 2001; Ferris et al., 2017; Fünfschilling et al., 2012; Korade and Kenworthy, 2008; X. Li et al., 2021). In addition to the role of exogenous cholesterol provided by glial cells, developing neurons heavily rely on their endogenous cholesterol biosynthesis, as a matter of fact, and this process is essential for their proper function and survival (Michikawa and Yanagisawa, 1999; Porter and Herman, 2011; Wang et al., 2021). Synaptic pruning and impaired development of neurons that occur with cholesterol deficiency may affect the efficiency of the auditory cortex in the auditory pathway and result in sensorineural hearing impairment.

Recent studies by Pechstein, A. et al. have demonstrated that SYN1 plays a crucial role in capturing small lipid vesicles into its phase, forming synapsin/liposome bio-condensates that contain clusters of small vesicles, whereas in the absence of SYN1, liposomes do not form such clusters (Milovanovic et al., 2018; Pechstein et al., 2020). The decrease of *Bcl2* simultaneously resulted in the loss of SYN1, which is most abundant in synaptic vesicles, and this presumably hindered the important function of synaptic proteins to capture lipid vesicles. This suggests that *Bcl2* may be involved in regulating the transport and localization of synaptic vesicles and, consequently, in the maintenance of synaptic function. It is reasonable to speculate whether *Bcl2* is participating in the capture of lipid vesicles by synaptic proteins that might affect the lipid metabolism of auditory cortical neurons. In addition, considering that glial cells under co-culture also assume responsibility for cholesterol synthesis (Wang et al., 2021), whether *Bcl2* has an impact on the nutrient delivery function and phagocytosis of glial cells is worth further investigation. *Bcl2* may be a key factor of metabolic homeostasis in the brain. In our in vitro study (cortical neuron), we employed *Bcl2* gene silencing (lower knockdown) to avoid excessive apoptotic effects. While the behaviors and responses observed in isolated cells in culture may differ significantly from those exhibited by intact organisms, the results obtained do provide valuable insights into the controlled environment of a petri dish. However, it is important to note that the knockdown was not performed in vivo, and the results may be influenced by the organism as a whole and its inherent complexity. To gain a more comprehensive understanding of the regulation of *Bcl2* in age-associated hearing damage, further investigations employing knockout animals and other means are warranted.

Immunohistochemistry analysis revealed that *Bcl2* exhibits specific localization in key regions of the auditory cortex, including the AUD and AUV, S1, and VLGMC and VLGPC. This specific localization suggests that *Bcl2* may have a specific role in these regions of the auditory cortex and may be involved in regulating synaptic function in these areas. We observed a decrease in *Bcl2* expression in the cortex of aged rats with increasing age, accompanied by a significant decrease in Map-2-labeled neuronal cytoskeletal protein associated with microtubules and a conspicuous shortening of synaptic length observed in the auditory conduction pathway and hippocampus. It has been shown that the mechanism for the *Bcl2* promotion of axonal growth is thought to be through the enhancement of intracellular Ca2+ signaling, which leads to the activation of CREB and extracellular regulated kinase (ERK), which are known to induce the expression of genes critical for neuronal growth and plasticity, resulting in the regulation of neuronal extension (Jiao et al., 2005).

The higher risk of dementia and AD in individuals with ARHL is likely associated with Bcl2 deficiency-induced degeneration in the hippocampus and nociceptors (Panza et al., 2015; Zhao et al., 2018). Studies have also investigated synaptic input from the medial geniculate (MGM) and the posterior ventral nucleus (PIN) cells to auditory cortical areas and highlighted the importance of presynaptic terminal and postsynaptic target features in their cortical areas, such as ADU and ADU, which plays an important role (Mellott et al., 2014; Peruzzi et al., 1997; Smith et al., 2019). *Bcl2* deletion is associated with synaptic dysfunction and neuropathy in ARHL. Our IF analysis of the cochlear basilar membrane showed that *Bcl2* deletion led to changes in hair cells, spiral ganglion cells, and nerve fiber density, which may contribute to neural obstruction in the cochlea and subsequent hearing loss in ARHL. These findings underscore the significant role of *Bcl2* as an important modulator of auditory synaptic function and neuropathy in the context of ARHL.

The auditory nerve comprises over 20,000 fibers that transmit sensory signals from the OHC and IHC to the brain (Buran et al., 2010). In the work by Bradley N. Buran et al., whole-cell capacitance measurements of IHCs in vitro revealed two components of depolarization-induced cellular extravasation (Peruzzi et al., 1997). The fast, transient component likely represents exocytosis of a limited pool of easily released vesicles, contributing to the rapid post-event adaptation of the AN response to sonic booms. The slower, sustained component may reflect vesicular replenishment of the active zone (Li et al., 2009; Meyer et al., 2016; Moser and Beutner, 2000; Schnee et al., 2005). The decline of *Bcl2* levels with age may impact synaptic activity in all auditory nerve

fibers, including the reduced number of fibers passing through the IHC and the observed shorter length. Consequently, decreasing *Bcl2* levels with age may interfere with normal auditory function.

Synaptic activity at all of these ANFs may be affected by decreasing *Bcl2* with age that interferes with normal function, including the reduced number of ANFs through the IHC and the shorter length that we have visualized. In established investigations, ARHL is often quantified using pure tone audiometry, which does not reflect the difficulty of speaking in noise or neurological ARHL in older adults, which may lead to an underestimation of the full impact of hearing loss on communication and daily living skills if not captured, which may lead to an underestimation of the association between hearing loss and cognitive decline (Meyer et al., 2016). The existing understanding of auditory perception and verbal communication in ARHL patients remains inadequate, particularly in studies that fail to explore the interplay between peripheral auditory, central auditory, and cognitive domains (Humes et al., 2012). Incorporating *Bcl2* levels as one of the criteria for ARHL screening could enhance its accuracy. The findings from this study suggest that targeting *Bcl2* may hold promise as a potential therapeutic intervention for ARHL. Further studies are warranted to elucidate the underlying mechanisms by which *Bcl2* regulates synaptic function and neuropathy in ARHL. Additionally, exploring potential therapeutic strategies that target *Bcl2* for ARHL treatment is crucial. Overall, our results provide novel insights into the molecular mechanisms underlying ARHL and propose *Bcl2* as a potential therapeutic target for ARHL.

It has been shown that oxidative stress arises from an imbalance between mitochondria-derived free radicals, including ROS and antioxidant enzymes, during the process of cellular senescence. This imbalance leads to activities such as oxidative protein modifications (Hauck et al., 2019) and lipid peroxidation of the plasma membrane (Sottero et al., 2018; Zarrouk et al., 2014), and consequently affects cellular viability. Particularly for the sensory cells such as cochlear hair cells, the plasma membrane characteristics of the OCHs are the essential conditions for the degree of sensitivity in transmitting the auditory signal (Ashmore, 2008; Hudspeth, 2008). In our study, we identified that *siBcl2* OC1 cells and neurons, with silenced *Bcl2* expression, exhibited an increased presence of 4-HNE (Fig. 7). Notably, IHCs play a pivotal role in auditory signal transmission, also showed a significantly elevation in 4-HNE levels and pronounced lipid peroxidation during the aging process in the aging cochlea of ARHL rats. An additional concern is that cells are constantly exposed to dangerous endogenous toxins during the survival process, such as the lipid peroxidation product 4-HNE that we have mentioned (Di Domenico et al., 2017; Hou et al., 2019). Cytochrome P450 (CYP) is one of the detoxification enzymes, accounting for 70–80% of all phase I detoxification enzymes. In humans, there are 57 CYP genes from 18 families, with all CYP5 family members primarily metabolizing endogenous toxins in a heavily substrate-specific manner (Nebert and Dalton, 2006). Our findings indicated a reduction in Cyp51 expression upon *Bcl2* silencing in OC1 cells (Fig. 3), which most probably indirectly exacerbates the accumulation of 4-HNE. Combined with our previous results, we propose that reduced *Bcl2* expression may induce lipid peroxidation of cell membranes, leading to oxidative stress and disruptions in lipid metabolism. These affects, in turn, affect the fluidity of plasma membranes in hair cells and neurons. We hypothesize that this pathway may represent a critical mechanism through which *Bcl2* modulates disease progression in ARHL.

In conclusion, this study provides important insights into the regulatory role of *Bcl2* in lipid metabolism, synaptic function, and neuropathy in the auditory cortex. It underscores the potential therapeutic significance of targeting *Bcl2* for the treatment of age-related hearing loss (ARHL). The findings highlight the critical involvement of *Bcl2* in maintaining the neurophysiological and neuropathological processes of the auditory cortex, particularly in the regulation of synaptic function in specific cortical regions. Moreover, this study emphasizes the importance of *Bcl2* in peripheral receptors during the aging process, as evidenced by the reduction in the number of ANFs in individual IHCs. Further research in this field holds the promise of revealing the underlying molecular mechanisms of ARHL and contribute to the development of innovative therapeutic approaches for this condition.

4. Key resources table

REAGENT or RESOURCE SOURCE IDENTIFIER
Antibodies
Rabbit anti-Bcl2 HUABIO Cat# ER0602
Mouse anti-Bcl2 HUABIO Cat# M1206–4
Rabbit anti-NeuN HUABIO Cat# ET1602–12
Rabbit anti-MAP-2 HUABIO Cat# HA500177
Rabbit anti-NSDHL HUABIO Cat# HA721088
Rabbit anti-CP51A HUABIO Cat# ER60263
Rabbit anti-LSS HUABIO Cat# HA500011
Rabbit anti-GAPDH HUABIO Cat# ET1601–4
Mouse anti-β-tubulin HUABIO Cat# EM0103
Rabbit anti-Neurofilament antibody Abcam Cat#ab207176
Rabbit anti-Synapsin I antibody Abcam Cat# ab254349
Mouse anti-MAP-2 Abcam Cat# ab300645
Mouse anti-PSD95 Abcam Cat# ab13552
Rabbit anti-4-HNE Bioss Bs-6313R
Anti-rabbit IgG, HRP-linked antibody Cell Signaling Technology Cat# 7074
Goat anti-mouse, Alexa Fluor 488 Invitrogen™ Cat# A-11001
Goat anti-rabbit, Alexa Fluor 488 Invitrogen™ Cat# A-11008
Goat anti-rabbit, Alexa Fluor 594 Invitrogen™ Cat# A-11012
Goat anti-mouse, Alexa Flour 647 Invitrogen™ Cat# A-21244
Chemicals, peptides, and recombinant proteins
DMEM Thermo Fisher Scientific Cat# 11995–065
Neurobasal Thermo Fisher Scientific Cat# 21103–049
Fetal Bovine Serum Procell Cat# 164210–50
B27 Thermo Fisher Scientific Cat# 17504–044
DAPI Solarbio Cat# C0065
Alexa Fluor™ 488 Phalloidin Invitrogen™ Cat# A12379
GlutaMAX Thermo Fisher Scientific Cat# 35050–61
Poly-ornithine Sigma-Aldrich Cat# P4957
Lipofectamine™ 3000 Thermo Fisher Scientific Cat# L3000001
TRIzol™ Reagent Thermo Fisher Scientific Cat# 15596018CN
Filipin III Apexbio Cat# B6034
DHE Abpbio Cat#C260
Trypsin-EDTA Thermo Fisher Scientific Cat# 25200056
Critical commercial assays
RT Master Mix for qPCR (gDNA digester plus) MedChemExpress Cat# HY-K0511
SYBR Green qPCR Master Mix (Low ROX) MedChemExpress Cat# HY-K0522
PAGE Gel Fast Preparation Kit Epizyme Cat# PG113
Experimental models: cell line
HEK293T the House Ear Institute, Los Angeles
OC1 the House Ear Institute, Los Angeles
Experimental models: organisms/strains
Sprague–Dawley rat GuangDong Medical Laboratory Animal Center
Software and algorithms
ImageJ NIH https://imagej.nih.gov/ij, RRID: SCR_003070
Prism 7 GraphPad Software https://www.graphpad.com/, RRID: SCR_002798

5. Method details

5.1. Cortical neuron culture

Cortical neurons were isolated from 0 to 3 days old SD rats in Hank's buffered salt solution, after Trypsin (Gibicol) dissociation, cells were resuspended in neuron culture media (neurobasal medium, B-27 supplement (200 ml/10 ml), 200 mM L-Glutamine, (Thermo Fisher Scientific), 50 units/ml penicillin, 50 μg/ml streptomycin). After standing for 10 min, we added the supernatant into the hole with 14 mm coverslips which coated with poly-L-lysine (Sigma-Aldrich; 1:4 in PBS). After 24 h of growth, replacing half of the plating medium by the same amount of new neuronal feeding medium with the same amount of fresh neuronal feeding medium. Henceforth culture media was changed every three days. Neurons were imaged with a Zeiss LSM880 Airyscan confocal microscope at DIV 9–10 and DIV 17–18.

5.2. Cell transfections

HEK-293 T cells and HEI-OC1 cells were placed into 6-well plates (3.0 × 105/ml) containing with 1 ml culture medium and 15 μl siRNA in Opti medium were used to transfected cells with 2 μl Lipo3000 per well. The targeting sequences were as follows: *Bcl2* siRNA1423(mus)5'-GGGAGAACAGGGUAUGAUATT-3′, *Bcl2* siRNA1928(mus) 5′- GGAUGACUGAGUACCUGAATT −3′. The cells were collected for total portein extraction and verification of cell function. In order to knock down the target gene-*Bcl2* of cortical neurons, we designed shRNAs by using ThermoFisher shRNA design tool. The targeting sequences were as follows: *Bcl2* shRNA 469(mouse) 5'-GGTATGATAACCGGGAGATCG-3′, *Bcl2* shRNA 470(mouse) 5'-GCTCTGTGGATGACTGAGTAC-3′ and *Bcl2* shRNA 471(mouse) 5'-GGATGGACCATGAAACAAAGT-3′, The synthesized shRNA oligos were inserted into double restriction sites (*Age*I and *Eco*RI) of plamid vector, and the recombinant plasmids were validate by sequencing. Lentiviral viruses of control and target shRNA vectors were used to infect HEK293T to collected and concentrated. 25 ml of *Bcl2* shRNA at titers of 2.57e+08 TU/ml were added into each chamber on first 24 h to infect cortical neurons. After 72 h infection, 1–2 μg/ml puromycin (10 μg/ml) was used to kill uninfected cells. To define the expression of target genes in control ang *Bcl2* knocked cells, qPCR and Western blot used to quantify the extent of the target gene deletion.

5.3. Immunofluorescence

For the quantization of plasticity and steroid metabolism, cortex neurons cultured to 10 and 17 days were fixed by 4% paraformaldehyde (PFA) in PBS for 15 min. After that neurons were washed three times in PBS and permeated with 0.5% Triton X-100 in PBS for 25 min at room temperature, then blocked with 10% normal goat serum in PBS for 1 h. After cells were incubated with primary antibody at 4 °C overnight, washed three times in PBS and next day incubated with secondary antibody at a room temperature for 1 h and DAPI for five minutes. Images were captured using Leica Application Suite X after immunofluorescence fixation and stained cells. Lentivirus-infected neurons with GFP green fluorescence dyes and confocal live cell imaging. ImageJ and Adobe Illustrator software serve as the tools for processing images and generating data.

5.4. Western blot and qPCR

Rat cortical neurons, HEI-OC1, and HEK293T cells were lysed in RIPA buffer which was added to protease inhibitor for 15 min and collected. The lysates were centrifuged at 12,000 rpm at 4 °C for 10 min. The supernatants were collected to perform Western blot with Rabbit anti-Bcl2 (1:1000, HUABIO), Rabbit anti-MAP-2 (1:500, HUABIO), Rabbit anti-NeuN (1:1000, HUABIO), Rabbit anti-NSDHL (1:200, HUABIO), Rabbit anti-LSS (1:500, HUABIO), Rabbit anti-CYP51A1 (1:500, HUABIO), Neurons cultured that transfected by lentivirus vector were washed once in PBS and scraped in Trizol (Thermo Fisher). Collected samples underwent RNA isolation using chloroform extraction and isopropanol precipitation. cDNA was synthesized from the RNA samples using RT Master Mix for qPCR (MedChemExpress). The qPCR reaction was performed using the SYBR Green qPCR Master Mix (MedChemExpress) according to manufacturer's instructions. Primers used for Nsdhl (5′- GTCAATTGGTTGCGCCAGAG) and (3′- ATCGACCTCAGCTTGCAGAC). Primers used for Lss were (5′- GTGGCAGAGAGTAGTGCTGT) and (3′- CAAAGAGTGGGCCTCTAGCC). Primers used for Cyp51 were (5′- GTTTCAGGCGCAGGGATAGA) and (3′- CATCTGTTAGAGGACGCCCG). Primers used for *Bcl2* were (5′- GCGTCAACAGGGAGATGTCA) and (3′- CCCAGAATCCACTCACACCC). Primers used for GAPDH were (5′-CCGCATCTTCTTGTGCAGTG) and (3′-ATGAAGGGGTCGTTGATGGC). Gene expression was calculated as normalized ratio and normalized to reference gene GAPDH using the AACt method.

5.5. Analysis of neuronal image

Within 5 μm of the cell body, dendrite thickness could be quantified at the base of dendrite by ImageJ. Drawing a series of concentric circles centered on the neuronal cell body for Sholl analysis by ImageJ Fiji. Counted every intersection of the control and *Bcl2* diminished groups that changes with distance from the cell body at each consecutive circle. Measuring length and shape of dendritic spines was also by ImageJ that classified into kinds of categories as mushroom, filopodia and stubby. Laser scanning confocal microscope (Leica, TCS SP8 X) took photos to collect neuronal cytoskeleton, morphology, synapses, dendritic branches and spine, with the use of same scanning parameters. 5 images at least from each group were captured for morphological analyses and selected to quantify spine numbers and classify spines.

5.6. RNA-seq analysis

Total RNA was qualified and quantified as follows: (1) RNA purity and concentration were then examined using NanoDrop 2000; (2) RNA integrity and quantity were measured using the Agilent 2100/4200 system. RNA library for RNA-seq was prepared as fllows: mRNA was purified from total RNA using polyT and then fragmented into 300–350 bp fragments, the first strand cDNA was reverse-transcribed using fragmented RNA and dNTPs (dATP, dTTP, dCTP and dGTP) and second strand cDNA synthesis was subsequently performed. Remaining overhangs of double-strand cDNA were converted into blunt ends via exonuclease/polymerase activities. After adenylation of 3′ ends of DNA fragments, sequencing adaptors were ligated to the cDNA and the library fragments were purified. The template was enriched by PCR, and the PCR product was purified to obtain the final library. After library preparation and pooling of different samples, the samples were subjected for Illumina sequencing. Commonly, the lncRNA-seq use PE150 (paired-end 150 nt) sequencing. EdgeR was used for differential expression analysis. The resulting *P*-values were adjusted using the Benjamini and Hochberg's approach for controlling the false discovery rate. Genes with $|\log2\ (\text{Fold Change})| > 1$ & q value <0.05 were assigned as differentially expressed. GO and KEGG enrichment analysis of differentially expressed gene sets were implemented by the top G (http://www.bioconductor.org/packages/release/bioc/html/topGO.html) and KOBAS(Bu et al., 2021) package, respectively. The experimental method is from Beijing Berry Genomics.

5.7. The immunofluorescence of cochlear

The cochlears of 8 M and 20 M SD rats were separated from the temporal bones and placed in 4% paraformaldehyde (PFA). The oval or round windows were punctured slightly for better preparation and removing the bony cartilage and excessive tissue to perform the fixation by 4% paraformaldehyde (PFA) in PBS for 18 h–24 h at 4 °C. The cochlear shell was decalcification after fixation in 10% EDTA for 24-36 h at 4 °C. The cochlear basilar membrane was dissected and permeated with 0.5% Triton X-100 in PBS for 25 min at room temperature, followed by blocking time was 30 min in 5%BSA. The segmented basilar membrane was proceeded on immunostaining with 1:200 dilution of anti-Neurofilament rabbit antibody (Abcam) and 1:100 dilution of anti-Bcl2 mouse antibody (HUABIO) overnight at 4 °C, and 4-HNE immunostaining used 1:200 dilution of anti-4HNE rabbit antibody (Bioss), followed by the incubation with Alexa-594 (Invitrogen), or Alexa-647 (Invitrogen) goat secondary antibodies and FITC-phalloidin the next day. Images were captured using Leica Application Suite X after mounting stained cochlear turns. ImageJ and Adobe Illustrator software serve as the tools for processing images and generating data.

5.8. Steroid metabolism assay

In order to measure cholesterol levels in neuron, we washed three

times with DPBS and fixed with 4% paraformaldehyde in PBS for 15 min, followed by permeabilization with 0.3% Triton X-100 in PBS for 15 min at room temperature. Cells were treated with filipin III(Apexbio) for 2 h and washed with DPBS. Fluorescence from cholesterol-bound filipin III was detected by microscope.

The neuronal cells we collected in sufficiently large numbers ($>1 \times 10^7$) from both control and treatment groups were prepared for performing metabolomics.The metabolites were extracted from cell residue with 1 mL precooled methanol/acetonitrile/water (*v*/v, 2:2:1) under sonication for 1 h in ice baths. The mixture was incubated at −20 °C for 1 h followed by centrifugation at 16,000 *g*, 4 °C for 20 min, and then transferred to the sampling vial for LC-MS analysis. The LC/MS portion of the platform was based on a Shimadzu Nexera X2 LC-30 CE system equipped with an Acquity UPLC HSS T3 column (1.8 μm 2.1 × 50 mm Column, Waters) and a triple quadruple mass spectrometer (5500 QTRAP, AB SCIEX). Metabolites were detected in electrospray negative-ionization and positive-ionization mode. The 5 μl samples were injected sequentially with LC autosampler. The Acquity UPLC HSS T3 column (1.8 μm 2.1 × 50 mm Column, Waters) was heated to 40 °C under a flow rate of 200 μl/min. A gradient was used to separate the compounds consisted of 0.1% Formic acid aqueous solution (solvent A) and 100% acetonitrile (solvent B). The gradient started at 100% solvent A for 2.5 min and increasing linearly to 70% solvent A over 9 min, and then increasing linearly to 0% solvent A over 1 min following with a 5.4 min hold before returning the starting mixture during 0.1 min and re-equilibrating for 2.5 min. QC samples were injected every several samples during acquisition. The MS conditions were set as follows: negative-ionization: Source Temperature 550 °C, Ion Source Gas1 (GAS1): 40, Ion Source Gas2 (GAS2): 50, Curtain Gas (CUR): 35, Ion Spray Voltage Floating (ISVF):-4500 V ; positive-ionization: Source Temperature 550 °C, Ion Source Gas1 (GAS1): 40, Ion Source Gas2 (GAS2): 50, Curtain Gas (CUR): 35, Ion Spray Voltage Floating (ISVF):5500 V. Transitions were detected by MRM mode.

MultiQuant 3.0.2 software was used to extract the original MRM data of MT1000 KIT metabolites and obtain the peak area of each metabolite. The discriminating metabolites were obtained using a statistically significant threshold of variable influence on projection (VIP) values obtained from the OPLS-DA model and two-tailed Student's *t*-test (*p* value) on the normalized raw data and randomize the samples in the data acquisition. The p value was calculated by one-way analysis of variance (ANOVA) for multiple groups analysis. Metabolites with VIP >1 and p value <0.05 were considered to be statistically significant metabolites. The experimental method is from ShangHai Bioprofile.

5.9. DHE probe detection of ROS

DHE probe was diluted with serum-free medium and added to live cells, the probe reacted with the cells for 5 min, then the medium was changed and the live cells were immediately photographed using the fluorescence microscope, and the fluorescence images were analyzed by ImageJ.

5.10. ELISA of 4-HNE

Accurately add 50 μl to the standard product on the enzyme label plate, add 40 μl to the sample diluent to the sample hole to be tested, and then 10 μl to the sample to be tested (the final dilution of the sample is 5 times). Add the sample to the bottom of the hole of the enzyme plate, try not to touch the hole wall, and gently shake and mix well. Warming: Use the sealing film to heat the plate at 37 °C for 30 min. Dispensing solution: dilute the 30 times concentrated washing liquid with distilled water 30 times and set aside. Washing: Carefully remove the sealing film, discard the liquid, shake it dry, fill each hole with washing liquid, let it sit for 30 s and then discard it, repeat 5 times and dry. Add enzyme: add 50 μl of enzyme label reagent to each pore, except for blank pores and warm again. After wash add the color developer A50μl to each hole first, then add the color developer B50μl, gently vibrate and mix well, and avoid light and color at 37 °C for 10 min. Termination: add 50 μl of termination liquid to each hole to terminate the reaction (at this time, the blue turns yellow. Measurement: Zero with blank holes and 450 nm wavelength to measure the absorbance (OD value) of each hole in sequence.

5.11. Statistical analysis and quantification

Data from 3 to 6 independent experiments were collected and summarized in Excel. Significance was defined as: "n.s." not significant or $p > 0.05$, for $p < 0.05$. Statistical tests include: One sample t-test, Mann-Whitney *U* test, Wilcoxon signed-rank test, Independent samples t-test, One-Way Anova with Tukey post-hoc. Statistical analyses of experimental date were performed by Prism 8 (GraphPad Software) to quantify as illustrations.

Author contributions

H. Zhang, and X. Zeng designed the study. Y. Liu, H. Zhang and C. Fan performed the analyses with assistance from Y. Liu, H. Zhang, S. Li, F. Liu, and J. Li contributed to experimental design, computational analyses, immunohistochemistry experiments, cell culture study, neuronal nuclei isolations, metabolomics experiments, mitochondrial related experiments and behavioral analyses in rat. Y. Liu, H. Zhang, and C. Fan wrote the manuscript. H. Zhang, and X. Zeng supervised the study. All authors discussed the results and interpretation, and contributed to the final version of the paper.

Open reseach

The RNAseq date obtained from this study was unload to the GEO database (https://www.ncbi.nlm.nih.gov/geo/) with accession number: GSE242359.

Ethics oversight

The care and use of animals and the experimental protocols (No.2021–0140) used in this study were approved by the Ethics Committee of ZSSOM under the Regulations for the Administration of Affairs Concerning Experimental Animals in China.

Acknowledgments and funding statement

Medical and Health Science and Technology Plan of Longgang Shenzhen (LGKCYLWS2022019, LGKCYLWS2022016). Shenzhen Science and Technology (JCYJ20210324142212033). The National Key Research and Development Program of China (2020YFB0204803), the Natural Science Foundation of China (81801132 and 81971190), Guangdong Key Field Research and Development Plan (2019B020228001 and 2018B010109006), and Natural Science Foundation of Guangzhou (2021A1515010256), and the Science and Technology Program of Guangzhou (201903010075), the National Key Research and Development Program of China (2020YFB020003), GD Frontier & Key Tech Innovation Program (2018B030337001).

Declaration of Competing Interest

The authors declare no competing interests.

Data availability

The data that supports the findings of this study are available in the supplementary material of this article. And some data that support the findings of this study are available from the corresponding author upon reasonable request.

Appendix A. Supplementary data

Supplementary data to this article can be found online at https://doi.org/10.1016/j.nbd.2023.106320.

References

Allman, B.L., Keniston, L.P., Meredith, M.A., 2009. Adult deafness induces somatosensory conversion of ferret auditory cortex. Proc. Natl. Acad. Sci. U. S. A. 106 (14), 5925–5930. https://doi.org/10.1073/pnas.0809483106.

Ashmore, J., 2008. Cochlear outer hair cell motility. Physiol. Rev. 88 (1), 173–210. https://doi.org/10.1152/physrev.00044.2006.

Awasthi, Y.C., Yang, Y., Tiwari, N.K., Patrick, B., Sharma, A., Li, J., Awasthi, S., 2004. Regulation of 4-hydroxynonenal-mediated signaling by glutathione S-transferases. Free Radic. Biol. Med. 37 (5), 607–619. https://doi.org/10.1016/j.freeradbiomed.2004.05.033.

Barres, B.A., Smith, S.J., 2001. Neurobiology. Cholesterol–making or breaking the synapse. Science 294 (5545), 1296–1297. https://doi.org/10.1126/science.1066724.

Brandt, A., Striessnig, J., Moser, T., 2003. CaV1.3 channels are essential for development and presynaptic activity of cochlear inner hair cells. J. Neurosci. 23 (34), 10832–10840. https://doi.org/10.1523/jneurosci.23-34-10832.2003.

Bu, D., Luo, H., Huo, P., Wang, Z., Zhang, S., He, Z., Kong, L., 2021. KOBAS-i: intelligent prioritization and exploratory visualization of biological functions for gene enrichment analysis. Nucleic Acids Res. 49 (W1), W317–w325. https://doi.org/10.1093/nar/gkab447.

Buckley, K.A., Tobey, E.A., 2011. Cross-modal plasticity and speech perception in pre- and postlingually deaf cochlear implant users. Ear Hear. 32 (1), 2–15. https://doi.org/10.1097/AUD.0b013e3181e8534c.

Buran, B.N., Strenzke, N., Neef, A., Gundelfinger, E.D., Moser, T., Liberman, M.C., 2010. Onset coding is degraded in auditory nerve fibers from mutant mice lacking synaptic ribbons. J. Neurosci. 30 (22), 7587–7597. https://doi.org/10.1523/jneurosci.0389-10.2010.

Campbell, J., Sharma, A., 2014. Cross-modal re-organization in adults with early stage hearing loss. PLoS One 9 (2), e90594. https://doi.org/10.1371/journal.pone.0090594.

Campbell, J., Sharma, A., 2016. Visual cross-modal re-Organization in Children with Cochlear implants. PLoS One 11 (1), e0147793. https://doi.org/10.1371/journal.pone.0147793.

Carpinelli, M.R., Wise, A.K., Arhatari, B.D., Bouillet, P., Manji, S.S., Manning, M.G., Burt, R.A., 2012. Anti-apoptotic gene Bcl2 is required for stapes development and hearing. Cell Death Dis. 3 (8), e362 https://doi.org/10.1038/cddis.2012.100.

Chang, C.C., Chang, Y.T., Huang, C.W., Tsai, S.J., Hsu, S.W., Huang, S.H., Lien, C.Y., 2018. Associations of Bcl2 rs956572 genotype groups in the structural covariance network in early-stage Alzheimer's disease. Alzheimers Res. Ther. 10 (1), 17. https://doi.org/10.1186/s13195-018-0344-4.

Chen, G.D., Zhao, H.B., 2007. Effects of intense noise exposure on the outer hair cell plasma membrane fluidity. Hear. Res. 226 (1–2), 14–21. https://doi.org/10.1016/j.heares.2006.06.007.

Cherko, M., Hickson, L., Bhutta, M., 2016. Auditory deprivation and health in the elderly. Maturitas 88, 52–57. https://doi.org/10.1016/j.maturitas.2016.03.008.

Chevy, F., Humbert, L., Wolf, C., 2005. Sterol profiling of amniotic fluid: a routine method for the detection of distal cholesterol synthesis deficit. Prenat. Diagn. 25 (11), 1000–1006. https://doi.org/10.1002/pd.1254.

Cosetti, M.K., Lalwani, A.K., 2015. Is cochlear implantation safe and effective in the elderly? Laryngoscope 125 (6), 1279–1281. https://doi.org/10.1002/lary.25055.

Dalleau, S., Baradat, M., Guéraud, F., Huc, L., 2013. Cell death and diseases related to oxidative stress: 4-hydroxynonenal (HNE) in the balance. Cell Death Differ. 20 (12), 1615–1630. https://doi.org/10.1038/cdd.2013.138.

Delbridge, A.R., Grabow, S., Strasser, A., Vaux, D.L., 2016. Thirty years of BCL2: translating cell death discoveries into novel cancer therapies. Nat. Rev. Cancer 16 (2), 99–109. https://doi.org/10.1038/nrc.2015.17.

Di Domenico, F., Tramutola, A., Butterfield, D.A., 2017. Role of 4-hydroxy-2-nonenal (HNE) in the pathogenesis of alzheimer disease and other selected age-related neurodegenerative disorders. Free Radic. Biol. Med. 111, 253–261. https://doi.org/10.1016/j.freeradbiomed.2016.10.490.

Eeles, E.M., White, S.V., O'Mahony, S.M., Bayer, A.J., Hubbard, R.E., 2012. The impact of frailty and delirium on mortality in older inpatients. Age Ageing 41 (3), 412–416. https://doi.org/10.1093/ageing/afs021.

Ferris, H.A., Perry, R.J., Moreira, G.V., Shulman, G.I., Horton, J.D., Kahn, C.R., 2017. Loss of astrocyte cholesterol synthesis disrupts neuronal function and alters whole-body metabolism. Proc. Natl. Acad. Sci. U. S. A. 114 (5), 1189–1194. https://doi.org/10.1073/pnas.1620506114.

Friedman, R.A., Van Laer, L., Huentelman, M.J., Sheth, S.S., Van Eyken, E., Corneveaux, J.J., Van Camp, G., 2009. GRM7 variants confer susceptibility to age-related hearing impairment. Hum. Mol. Genet. 18 (4), 785–796. https://doi.org/10.1093/hmg/ddn402.

Frisina, R.D., Ding, B., Zhu, X., Walton, J.P., 2016. Age-related hearing loss: prevention of threshold declines, cell loss and apoptosis in spiral ganglion neurons. Aging (Albany NY) 8 (9), 2081–2099. https://doi.org/10.18632/aging.101045.

Fünfschilling, U., Jockusch, W.J., Sivakumar, N., Möbius, W., Corthals, K., Li, S., Saher, G., 2012. Critical time window of neuronal cholesterol synthesis during neurite outgrowth. J. Neurosci. 32 (22), 7632–7645. https://doi.org/10.1523/jneurosci.1352-11.2012.

Giroud, N., Lemke, U., Reich, P., Matthes, K.L., Meyer, M., 2017. The impact of hearing aids and age-related hearing loss on auditory plasticity across three months - an electrical neuroimaging study. Hear. Res. 353, 162–175. https://doi.org/10.1016/j.heares.2017.06.012.

Gopinath, B., Rochtchina, E., Wang, J.J., Schneider, J., Leeder, S.R., Mitchell, P., 2009. Prevalence of age-related hearing loss in older adults: Blue Mountains study. Arch. Intern. Med. 169 (4), 415–416. https://doi.org/10.1001/archinternmed.2008.597.

Gu, Z., Serradj, N., Ueno, M., Liang, M., Li, J., Baccei, M.L., Yoshida, Y., 2017. Skilled movements require non-apoptotic Bax/Bak pathway-mediated corticospinal circuit reorganization. Neuron 94 (3), 626–641.e624. https://doi.org/10.1016/j.neuron.2017.04.019.

Hauck, A.K., Huang, Y., Hertzel, A.V., Bernlohr, D.A., 2019. Adipose oxidative stress and protein carbonylation. J. Biol. Chem. 294 (4), 1083–1088. https://doi.org/10.1074/jbc.R118.003214.

He, D., Li, L., Lu, Z., Li, S., Lan, T., Liu, F., Zhao, H., 2023. Integrating gene mutation spectra from tumors and the general population with gene expression topological networks to identify novel cancer driver genes. BioRxiv 2023, 539093. https://doi.org/10.1101/2023.05.02.539093.

Hogan, A., O'Loughlin, K., Miller, P., Kendig, H., 2009. The health impact of a hearing disability on older people in Australia. J. Aging Health 21 (8), 1098–1111. https://doi.org/10.1177/0898264309347821.

Hou, Y., Dan, X., Babbar, M., Wei, Y., Hasselbalch, S.G., Croteau, D.L., Bohr, V.A., 2019. Ageing as a risk factor for neurodegenerative disease. Nat. Rev. Neurol. 15 (10), 565–581. https://doi.org/10.1038/s41582-019-0244-7.

Hudspeth, A.J., 2008. Making an effort to listen: mechanical amplification in the ear. Neuron 59 (4), 530–545. https://doi.org/10.1016/j.neuron.2008.07.012.

Humes, L.E., Dubno, J.R., Gordon-Salant, S., Lister, J.J., Cacace, A.T., Cruickshanks, K.J., Wingfield, A., 2012. Central presbycusis: a review and evaluation of the evidence. J. Am. Acad. Audiol. 23 (8), 635–666. https://doi.org/10.3766/jaaa.23.8.5.

Jiao, S., Li, Z., 2011. Nonapoptotic function of BAD and BAX in long-term depression of synaptic transmission. Neuron 70 (4), 758–772. https://doi.org/10.1016/j.neuron.2011.04.004.

Jiao, J., Huang, X., Feit-Leithman, R.A., Neve, R.L., Snider, W., Dartt, D.A., Chen, D.F., 2005. Bcl2 enhances ca(2+) signaling to support the intrinsic regenerative capacity of CNS axons. EMBO J. 24 (5), 1068–1078. https://doi.org/10.1038/sj.emboj.7600589.

Kalra, G., Milon, B., Casella, A.M., Herb, B.R., Humphries, E., Song, Y., Ament, S.A., 2020. Biological insights from multi-omic analysis of 31 genomic risk loci for adult hearing difficulty. PLoS Genet. 16 (9), e1009025 https://doi.org/10.1371/journal.pgen.1009025.

Keithley, E.M., Feldman, M.L., 1982. Hair cell counts in an age-graded series of rat cochleae. Hear. Res. 8 (3), 249–262. https://doi.org/10.1016/0378-5955(82)90017-x.

Kim, M.B., Shim, H.Y., Jin, S.H., Kang, S., Woo, J., Han, J.C., Hong, S.H., 2016. Cross-modal and intra-modal characteristics of visual function and speech perception performance in Postlingually deafened, cochlear implant users. PLoS One 11 (2), e0148466. https://doi.org/10.1371/journal.pone.0148466.

Korade, Z., Kenworthy, A.K., 2008. Lipid rafts, cholesterol, and the brain. Neuropharmacology 55 (8), 1265–1273. https://doi.org/10.1016/j.neuropharm.2008.02.019.

Li, G.L., Keen, E., Andor-Ardó, D., Hudspeth, A.J., von Gersdorff, H., 2009. The unitary event underlying multiquantal EPSCs at a hair cell's ribbon synapse. J. Neurosci. 29 (23), 7558–7568. https://doi.org/10.1523/jneurosci.0514-09.2009.

Li, X., Zhang, J., Li, D., He, C., He, K., Xue, T., Liu, Q., 2021. Astrocytic ApoE reprograms neuronal cholesterol metabolism and histone-acetylation-mediated memory. Neuron 109 (6), 957–970.e958. https://doi.org/10.1016/j.neuron.2021.01.005.

Lin, F.R., Thorpe, R., Gordon-Salant, S., Ferrucci, L., 2011. Hearing loss prevalence and risk factors among older adults in the United States. J. Gerontol. A Biol. Sci. Med. Sci. 66 (5), 582–590. https://doi.org/10.1093/gerona/glr002.

Maulucci, G., Troiani, D., Eramo, S.L., Paciello, F., Podda, M.V., Paludetti, G., Fetoni, A. R., 2014. Time evolution of noise induced oxidation in outer hair cells: role of NAD (P)H and plasma membrane fluidity. Biochim. Biophys. Acta 1840 (7), 2192–2202. https://doi.org/10.1016/j.bbagen.2014.04.005.

Mellott, J.G., Foster, N.L., Ohl, A.P., Schofield, B.R., 2014. Excitatory and inhibitory projections in parallel pathways from the inferior colliculus to the auditory thalamus. Front. Neuroanat. 8, 124. https://doi.org/10.3389/fnana.2014.00124.

Meyer, C., Grenness, C., Scarinci, N., Hickson, L., 2016. What is the international classification of functioning, disability and health and why is it relevant to audiology? Semin. Hear. 37 (3), 163–186. https://doi.org/10.1055/s-0036-1584412.

Michikawa, M., Yanagisawa, K., 1999. Inhibition of cholesterol production but not of nonsterol isoprenoid products induces neuronal cell death. J. Neurochem. 72 (6), 2278–2285. https://doi.org/10.1046/j.1471-4159.1999.0722278.x.

Milovanovic, D., Wu, Y., Bian, X., De Camilli, P., 2018. A liquid phase of synapsin and lipid vesicles. Science 361 (6402), 604–607. https://doi.org/10.1126/science.aat5671.

Moser, T., Beutner, D., 2000. Kinetics of exocytosis and endocytosis at the cochlear inner hair cell afferent synapse of the mouse. Proc. Natl. Acad. Sci. U. S. A. 97 (2), 883–888. https://doi.org/10.1073/pnas.97.2.883.

Moser, T., Starr, A., 2016. Auditory neuropathy–neural and synaptic mechanisms. Nat. Rev. Neurol. 12 (3), 135–149. https://doi.org/10.1038/nrneurol.2016.10.

Mykytczuk, N.C., Trevors, J.T., Leduc, L.G., Ferroni, G.D., 2007. Fluorescence polarization in studies of bacterial cytoplasmic membrane fluidity under environmental stress. Prog. Biophys. Mol. Biol. 95 (1–3), 60–82. https://doi.org/10.1016/j.pbiomolbio.2007.05.001.

Nebert, D.W., Dalton, T.P., 2006. The role of cytochrome P450 enzymes in endogenous signalling pathways and environmental carcinogenesis. Nat. Rev. Cancer 6 (12), 947–960. https://doi.org/10.1038/nrc2015.

Nevado, J., Sanz, R., Casqueiro, J.C., Ayala, A., García-Berrocal, J.R., Ramírez-Camacho, R., 2006. Ageing evokes an intrinsic pro-apoptotic signalling pathway in rat cochlea. Acta Otolaryngol. 126 (11), 1134–1139. https://doi.org/10.1080/00016480600672592.

Nikolaev, A., McLaughlin, T., O'Leary, D.D., Tessier-Lavigne, M., 2009. APP binds DR6 to trigger axon pruning and neuron death via distinct caspases. Nature 457 (7232), 981–989. https://doi.org/10.1038/nature07767.

Ohsawa, S., Hamada, S., Kuida, K., Yoshida, H., Igaki, T., Miura, M., 2010. Maturation of the olfactory sensory neurons by Apaf-1/caspase-9-mediated caspase activity. Proc. Natl. Acad. Sci. U. S. A. 107 (30), 13366–13371. https://doi.org/10.1073/pnas.0910488107.

Panza, F., Solfrizzi, V., Frisardi, V., Maggi, S., Sancarlo, D., Adante, F., Pilotto, A., 2011. Different models of frailty in predementia and dementia syndromes. J. Nutr. Health Aging 15 (8), 711–719. https://doi.org/10.1007/s12603-011-0126-1.

Panza, F., Solfrizzi, V., Logroscino, G., 2015. Age-related hearing impairment-a risk factor and frailty marker for dementia and AD. Nat. Rev. Neurol. 11 (3), 166–175. https://doi.org/10.1038/nrneurol.2015.12.

Pechstein, A., Tomilin, N., Fredrich, K., Vorontsova, O., Sopova, E., Evergren, E., Shupliakov, O., 2020. Vesicle clustering in a living synapse depends on a Synapsin region that mediates phase separation. Cell Rep. 30 (8), 2594–2602.e2593. https://doi.org/10.1016/j.celrep.2020.01.092.

Peruzzi, D., Bartlett, E., Smith, P.H., Oliver, D.L., 1997. A monosynaptic GABAergic input from the inferior colliculus to the medial geniculate body in rat. J. Neurosci. 17 (10), 3766–3777. https://doi.org/10.1523/jneurosci.17-10-03766.1997.

Pfrieger, F.W., 2003. Role of cholesterol in synapse formation and function. Biochim. Biophys. Acta 1610 (2), 271–280. https://doi.org/10.1016/s0005-2736(03)00024-5.

Pieribone, V.A., Shupliakov, O., Brodin, L., Hilfiker-Rothenfluh, S., Czernik, A.J., Greengard, P., 1995. Distinct pools of synaptic vesicles in neurotransmitter release. Nature 375 (6531), 493–497. https://doi.org/10.1038/375493a0.

Porter, F.D., Herman, G.E., 2011. Malformation syndromes caused by disorders of cholesterol synthesis. J. Lipid Res. 52 (1), 6–34. https://doi.org/10.1194/jlr.R009548.

Ren, F., Ma, W., Li, M., Sun, H., Xin, Q., Zong, W., Zhao, B., 2018. Gray matter atrophy is associated with cognitive impairment in patients with Presbycusis: a comprehensive morphometric study. Front. Neurosci. 12, 744. https://doi.org/10.3389/fnins.2018.00744.

Rigters, S.C., Bos, D., Metselaar, M., Roshchupkin, G.V., Baatenburg de Jong, R.J., Ikram, M.A., Goedegebure, A., 2017. Hearing impairment is associated with smaller brain volume in aging. Front. Aging Neurosci. 9, 2. https://doi.org/10.3389/fnagi.2017.00002.

Robertson, D.A., Savva, G.M., Kenny, R.A., 2013. Frailty and cognitive impairment–a review of the evidence and causal mechanisms. Ageing Res. Rev. 12 (4), 840–851. https://doi.org/10.1016/j.arr.2013.06.004.

Rutherford, M.A., Chapochnikov, N.M., Moser, T., 2012. Spike encoding of neurotransmitter release timing by spiral ganglion neurons of the cochlea. J. Neurosci. 32 (14), 4773–4789. https://doi.org/10.1523/jneurosci.4511-11.2012.

Sanz-Fernández, R., Sánchez-Rodriguez, C., Granizo, J.J., Durio-Calero, E., Martín-Sanz, E., 2016. Accuracy of auditory steady state and auditory brainstem responses to detect the preventive effect of polyphenols on age-related hearing loss in Sprague-Dawley rats. Eur. Arch. Otorhinolaryngol. 273 (2), 341–347. https://doi.org/10.1007/s00405-015-3551-7.

Schnee, M.E., Lawton, D.M., Furness, D.N., Benke, T.A., Ricci, A.J., 2005. Auditory hair cell-afferent fiber synapses are specialized to operate at their best frequencies. Neuron 47 (2), 243–254. https://doi.org/10.1016/j.neuron.2005.06.004.

Shiell, M.M., Champoux, F., Zatorre, R.J., 2016. The right hemisphere Planum Temporale supports enhanced visual motion detection ability in deaf people: evidence from cortical thickness. Neural Plast. 2016, 7217630. https://doi.org/10.1155/2016/7217630.

Shimohama, S., Fujimoto, S., Sumida, Y., Tanino, H., 1998. Differential expression of rat brain Bcl2 family proteins in development and aging. Biochem. Biophys. Res. Commun. 252 (1), 92–96. https://doi.org/10.1006/bbrc.1998.9577.

Simon, D.J., Weimer, R.M., McLaughlin, T., Kallop, D., Stanger, K., Yang, J., Tessier-Lavigne, M., 2012. A caspase cascade regulating developmental axon degeneration. J. Neurosci. 32 (49), 17540–17553. https://doi.org/10.1523/jneurosci.3012-12.2012.

Slade, K., Plack, C.J., Nuttall, H.E., 2020. The effects of age-related hearing loss on the brain and cognitive function. Trends Neurosci. 43 (10), 810–821. https://doi.org/10.1016/j.tins.2020.07.005.

Smith, P.H., Uhlrich, D.J., Manning, K.A., 2019. Evaluation of medial division of the medial geniculate (MGM) and posterior intralaminar nucleus (PIN) inputs to the rat auditory cortex, amygdala, and striatum. J. Comp. Neurol. 527 (9), 1478–1494. https://doi.org/10.1002/cne.24644.

Sottero, B., Rossin, D., Poli, G., Biasi, F., 2018. Lipid oxidation products in the pathogenesis of inflammation-related gut diseases. Curr. Med. Chem. 25 (11), 1311–1326. https://doi.org/10.2174/0929867324666170619104105.

Stropahl, M., Plotz, K., Schönfeld, R., Lenarz, T., Sandmann, P., Yovel, G., Debener, S., 2015. Cross-modal reorganization in cochlear implant users: auditory cortex contributes to visual face processing. Neuroimage 121, 159–170. https://doi.org/10.1016/j.neuroimage.2015.07.062.

Taljaard, D.S., Olaithe, M., Brennan-Jones, C.G., Eikelboom, R.H., Bucks, R.S., 2016. The relationship between hearing impairment and cognitive function: a meta-analysis in adults. Clin. Otolaryngol. 41 (6), 718–729. https://doi.org/10.1111/coa.12607.

Tekpli, X., Holme, J.A., Sergent, O., Lagadic-Gossmann, D., 2013. Role for membrane remodeling in cell death: implication for health and disease. Toxicology 304, 141–157. https://doi.org/10.1016/j.tox.2012.12.014.

Wang, H., Kulas, J.A., Wang, C., Holtzman, D.M., Ferris, H.A., Hansen, S.B., 2021. Regulation of beta-amyloid production in neurons by astrocyte-derived cholesterol. Proc. Natl. Acad. Sci. U. S. A. 118 (33) https://doi.org/10.1073/pnas.2102191118.

Zarrouk, A., Vejux, A., Mackrill, J., O'Callaghan, Y., Hammami, M., O'Brien, N., Lizard, G., 2014. Involvement of oxysterols in age-related diseases and ageing processes. Ageing Res. Rev. 18, 148–162. https://doi.org/10.1016/j.arr.2014.09.006.

Zeng, M., Shang, Y., Araki, Y., Guo, T., Huganir, R.L., Zhang, M., 2016. Phase transition in postsynaptic densities underlies formation of synaptic complexes and synaptic plasticity. Cell 166 (5), 1163–1175.e1112. https://doi.org/10.1016/j.cell.2016.07.008.

Zhang, H., Fan, C., Li, L., Liu, F., Li, S., Ma, L., Zhao, H., 2023. Repurposing the memory-promoting Meclofenoxate hydrochloride as a treatment for Parkinson's disease through integrative multi-omics analysis. BioRxiv 2023, 53602. https://doi.org/10.1101/2023.04.07.536024.

Zhao, N., Liu, C.C., Qiao, W., Bu, G., 2018. Apolipoprotein E, receptors, and modulation of Alzheimer's disease. Biol. Psychiatry 83 (4), 347–357. https://doi.org/10.1016/j.biopsych.2017.03.003.